Efficiency Improvement for III-V Nitride Micro Light-Emitting Diodes

by

Jian Yin

A thesis

presented to the University of Waterloo

in fulfilment of the

thesis requirement for the degree of

Master of Applied Science

in

Electrical and Computer Engineering

Waterloo, Ontario, Canada, 2019

Author’s Declaration

I hereby declare that I am the sole author of this thesis. This is a true copy of the thesis, including any required final revisions, as accepted by my examiners.

I understand that my thesis may be made electronically available to the public.

Abstract

As a solid-state lighting source with high luminance and long life-time, the gallium nitride/ indium gallium nitride (GaN/InGaN) light-emitting diode (LED) is considered as a promising technology for many applications, including opto-genetic neuromodulation, micro-indicators and self-emissive micro-displays. The biggest technical challenge with conventional GaN/InGaN LEDs is the so-called efficiency droop, which is mainly attributed to three reasons: Auger recombination, low hole injection and carrier overflow. On the contrary, the substantial carrier loss due to Shockley–Read–Hall (SRH) surface recombination is usually ignored in conventional GaN/InGaN LEDs. However, when the size of the GaN/InGaN LEDs shrinks down to a few micrometers, the increased surface area to volume ratio leads to a high carrier surface recombination rate, which significantly degrades the efficiency performance of GaN/InGaN micro-LEDs (μ-LEDs). In this case, the surface recombination velocity (SRV), which reflects the impact of surface recombination rate, becomes the most critical parameter affecting the device performance.

This thesis investigates the surface recombination impacts on the efficiency performance of size-dependent GaN/InGaN μ-LEDs. In this work, the simulation tool APSYS crosslight is employed to simulate GaN-based μ-LEDs by setting the SRV to 3×10^4 cm/s at room temperature. The simulation results show that the internal quantum efficiency of μ-LEDs decreases from 53% to 4% when the size shrinks down from 100μm to 5μm. The simulation results are then confirmed with the temperature-dependent experimental data measured on 50×50 μm^2 μ-LEDs. Further investigation shows GaN/InGaN μ-LEDs with n-doped quantum barriers significantly improved the efficiency of LEDs in common working current density range.

Based on the modeling results, a new design of GaN/InGaN μ-LEDs with n-doped quantum barriers are proposed to improve the efficiency in GaN/InGaN μ-LEDs with small sizes (<10μm in dimension). For GaN/InGaN μ-LEDs with n-doped quantum barriers, calculation shows that the SRH recombination rate (surface recombination) in the n-GaN is much smaller than the p-GaN. By considering the tradeoff between balance of electron-hole injection and suppressing surface recombination, an optimized 5×5 μm^2 GaN/InGaN μ-LEDs with n-doped quantum barriers and single quantum well design is presented. The estimated efficiency of the new design is two times higher than that in conventional intrinsic multiple quantum wells based μ-LEDs.

Acknowledgements

I would like to thank my supervisor Prof. Dayan Ban for his patience and encouragement throughout my Master studies. This work would not have been possible without his support and guidance.

I want to express my gratitude to the readers of this thesis, Prof. Guo-Xing Miao and Prof. Bo Cui.

My deepest gratitude goes to Dr. Chao Xu, Dr. Shazzad Rassel, Dr. Ehsanollah Fathi, Dr. Hossein Zamani Siboni, and Mr. Boyu Wen for sharing their research experience with me.

I would like to thank my friend, Zongxian, Xiaoliang, Yutong, Yixiao, Yue and Boyu, for their encouragement and company, when I feel depressed and lonely.

This work would not have been finished without the help and support of my colleagues. I would like to express my gratitude to Chao, Boyu, Xiaoliang, Yue, Siyi, Alam, Asif, Cathy, Burak and Masud for their company and interesting discussions during my Master studies. It is my pleasure to work with them and I really enjoy it.

Finally, I must express my very profound gratitude to my parents and my uncle, for all the mental and financial support throughout all those years. This accomplishment would not have been possible without the support from my family. Thank you.

Table of Contents

List of Figures

List of Tables

List of Abbreviations

LED	Light-emitting diode
μ-LED	Micro light-emitting diode
OLED	Organic light-emitting diode
LCD	Liquid crystal display
CCFL	Cold-cathode fluorescent lamp
RGB	Red, green and blue
IQE	Internal quantum efficiency
EQE	External quantum efficiency
EL	Electroluminescence
TADF	Thermal activated delay fluorescence
RISC	Reverse intersystem crossing
SRH	Shockley-Read-Hall
QW	Quantum well
MQW	Multiple quantum well
EBL	Electron blocking layer
SRV	Surface recombination velocity

Chapter 1 Introduction

1.1 Background and Motivation

In 1961, Dr. James R. Biard and Gary Pittman, who were employees at Texas Instruments, accidentally discovered near-infrared light emission from an Esaki diode they had constructed on a gallium arsenide (GaAs) semi-insulating substrate. These two inventors filed a patent titled "Semiconductor Radiant Diode", which consist of a zinc-diffused p–n junction GaAs light-emitting diode (LED) with a spaced cathode contact on the tin-doped N-type regrowth layer to allow high-efficiency emission under forward bias. This should be the first practical LED in the world (shown in Figure 1.1).[1]. Afterwards the red,[2] yellow [3] and blue [4] LEDs were invented in the 1970s. Fairchild Optoelectronics was the first commercial and successful firm to produce most low-cost LEDs.[3] With the advance of technology, 40 years after, LEDs of different colors, especially white light, have gradually replaced the incandescent light sources used in various lighting application and LED displays.

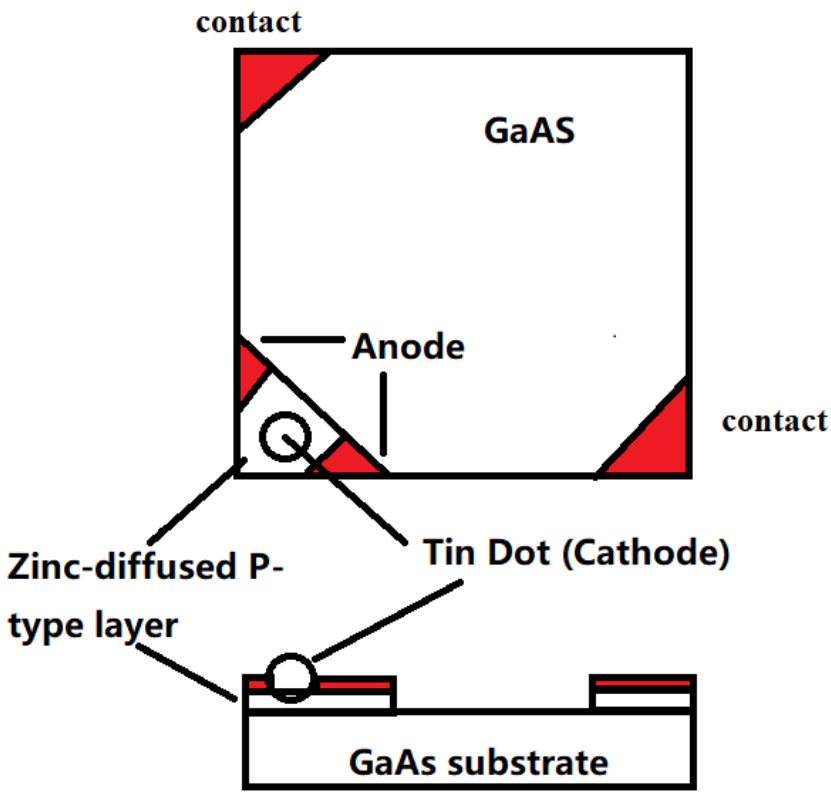

Figure 1.1 Diagram of the first practical LED. [1]

The LED display includes an array of LEDs as pixels and each pixel is an individual LED device. As the pursuit for resolution and brightness of video equipment increases, it was necessary to scale down the LED displays and optimize the efficiency to adapt to ongoing demands. Liquid crystal displays (LCDs), organic LEDs (OLEDs) and micro LEDs (μ-LEDs), are three mainstream technologies for micro-display in future. Compared to the LCDs and OLEDs, the μ-LED displays have lots of advantages on luminance, response time, life-time and contrast ratio. It promises to be the best new-generation display technology with great potential, but production still faces many challenges. Despite the high cost of fabrication, the major challenge of the μ-LEDs remains the efficiency droop. For LEDs with bigger sizes, the efficiency droop describes the phenomenon when the efficiency starts to decrease as the injected current density becomes higher. This problem can be mainly attributed to three reasons: Auger recombination, [5,6] carrier overflow [7,8] and low hole injection. [9,10] Moreover, in μ-LEDs, when the size shrinks down to a few micrometers, the high surface areas to volumes ratio leads to a high surface recombination, which plays a critical role in the efficiency performance of the gallium nitride/ indium gallium nitride (GaN/InGaN) based μ-LEDs. [11-13] This thesis is aimed at improving the efficiency of blue light GaN/InGaN μ-LEDs by analyzing how surface recombination impacts on the efficiency performance of size-dependent GaN/InGaN μ-LEDs, and further proposes some high-efficiency LED designs.

1.2 Literature Review

1.2.1 Light-Emitting Diode

LEDs are semiconductor light material sources that combine a P-type semiconductor layer with high hole concentration to a N-type semiconductor layer with high electron concentration. Applying a sufficient forward voltage leads the electrons and holes to recombine at the P-N junction, resulting in a near bandgap radiation. The early LED structures were mainly homojunction semiconductor structures (shown in Figure 1.2).

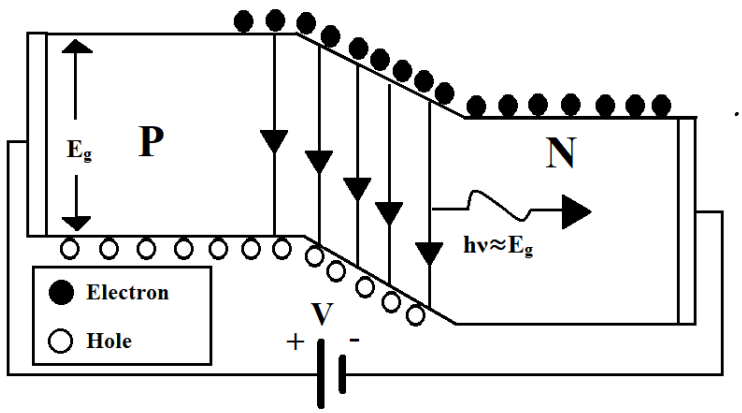

Figure 1.2 Diagram of the homojunction LED structure.

Although it is much easier to fabricate homojunction semiconductor structures, most researchers still adopt the heterojunction semiconductor structure as LED structures. There are two advantages of using heterojunction structures. [14] One advantage is that it increases the carrier injection efficiency by using the quantum well (QW) structure (shown in Figure 1.3), which is a special kind of heterojunction structure. The electrons and holes in the QW are confined in a one-dimension or quasi-two-dimensional space and lead to the discrete energy levels. This quantum confinement effect, due to the thin QW layers, generates a very high injection efficiency in LEDs. Another advantage is the clever use of wide-bandgap materials. The wide-bandgap quantum barriers are transparent to the photons generated in the narrow-bandgap QW layers and reduces the photon reabsorption. The light emitted from the QW layers can go in an arbitrary direction. Therefore, a common separate LED with hemispherical- dome shape is made on the top, which acts as a lens to focus the light upwards.

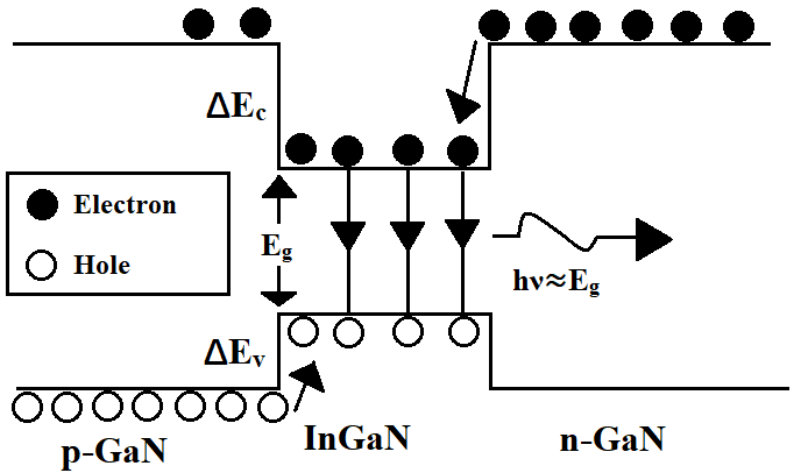

Figure 1.3 Diagram of the heterojunction LED band structure (Take GaN/InGaN as an example).

1.2.2 Materials for different colors LEDs

The energy bandgap of the semiconductor materials determines the wavelength of the emitted light. For a homojunction structure LED, the wavelength is given by:

$$\lambda_0 = \frac{1.24}{E_{gap}}[\mu m] \quad (1.1),$$

For a QW structure with the same emitted material, the electrons and holes recombine from the subbands and the emission is blue shifted, which means the wavelength of the emitted light is shorter than the λ_0. For achieving different color, we need different materials with different energy band gaps as emitted materials. Table 1 shows the inorganic semiconductor materials and the luminescent color of the respective LEDs: [3]

Color	Wavelength Range	Semiconductor Material
Infrared	>760 nm	GaAs, AlGaAs
Red	610-760 nm	AlGaAs, GaAsP, AlGaInP
Amber/Yellow	570-610 nm	GaAsP, AlGaInP, GaP
Green	500-570 nm	InGaN, AlGaInP, GaP, AlGaP
Blue	450-500 nm	ZnSe, InGaN, SiC
Violet	380-450 nm	InGaN
ultraviolet	<380 nm	C (diamond), AlN, AlGaN, AlGaInN

Table 1.1 The different semiconductor materials for different colors of LEDs

Besides these colors, the white LEDs has become more important and has replaced the colored LEDs for lighting application and LED displays. Since white light is not monochromatic, there are two methods to generate white LED. One method is the combination of three monochromatic LEDs (red, green and blue LEDs). The spectrum of this kind of white LEDs includes three narrow bands, which results in bad color rendering. Therefore, the popular method nowadays is coating one or few layers of the fluorescent agent to convert the blue or violet light monochromatic LEDs to red, green or yellow colors. The combination of these colors with remaining blue or violet light appears as white to the human eyes. [4] As we mentioned earlier, before 1972, researchers have already made red, yellow and blue LEDs. However, the luminance of initial blue LEDs made of p-GaN (Mg-doped GaN) was too weak for practical use. Therefore, until Dr. Nakamura Shuji made the high luminance blue InGaN based LED, [15,16] there were no commercial blue or white LEDs in the world. The high efficiency and low cost of InGaN based LEDs is the reason why it remained the most valued LEDs.

1.2.3 LED-backlit Liquid Crystal Display

After the third industrial revolution, almost every invention was inseparable from modern computers. Most of the modern computers carry output devices, like monitors or cellphone screens. Before the popularity of the OLED displays, most screens were the LCD type. The structure of an LCD is shown in Figure 1.4. The liquid crystal layer sits between two polarizers in a twisted phase and can reorient the light from the first polarizer so it can pass through the second polarizer. When an electric field is applied to the liquid crystal layer through the electrode, the LC layer untwists and becomes perpendicular to the polarizers. In this situation, the LC layer cannot reorient the light from the first polarizer, which will be blocked by the second polarizer. This way, each pixel of LCD can be turned on or off, and because the colors of LCD are generated by color filters, a white light source is generally needed.

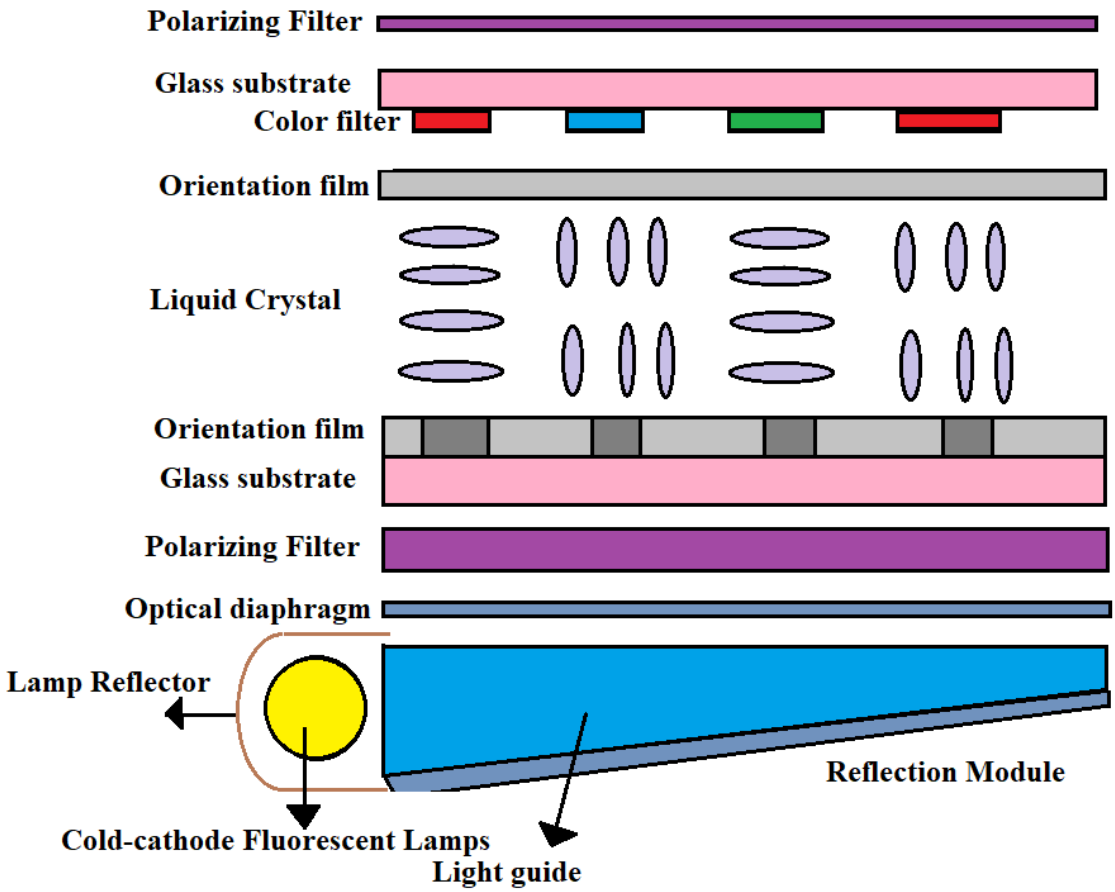

Figure 1.4 Diagram of the liquid crystal display structure.

Before the invention of practical white LEDs, the cold-cathode fluorescent lamps (CCFLs) were used as the light source in LCDs. However, with the emergence of the high-efficiency white LEDs, CCFLs were gradually replaced as the light source in LCD. For a better distinction, the LCDs using white LEDs or red, green and blue (RGB) LEDs as the light source is called LED-backlit LCD. There are two types of LED-backlit LCDs based on the different arrangement of the LED. One type is called direct back-lit arrangement, where the LEDs are arrayed directly behind the screen as back-light source. The other type is called edge-lit LED arrangement, where the LEDs averagely sit at the edge of a screen with a special reflector (light guide) to reflect the light evenly to the screen. These two types of LED-backlit LCD have different advantages. The former has wider color gamut while the latter has less thickness. LED-backlit LCDs are widely used in TVs, computer screens and large high definition displays.

1.2.4 Organic LED

LED-backlit LCD using LEDs as backlight source is strictly not an LED displays. Nowadays,

OLEDs are used in small and high-resolution LED displays such as cellphone screens. The structure of an OLED is shown in Figure 1.5.

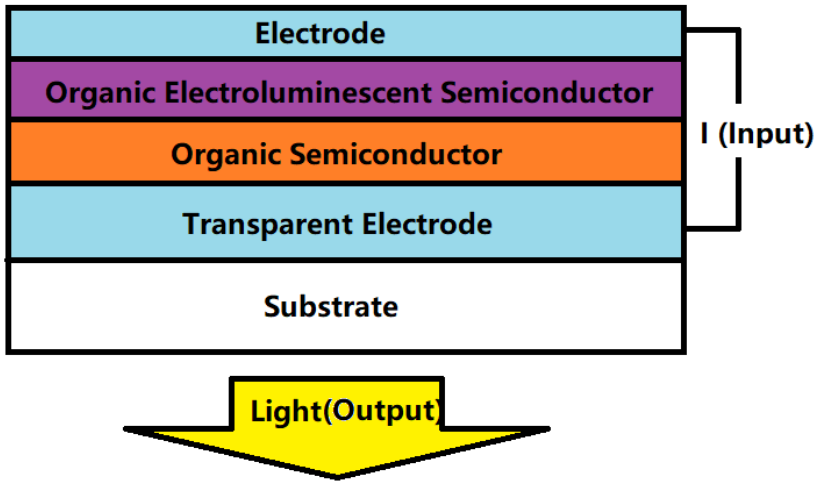

Figure 1.5 The diagram of OLED structure.

The main advantages of OLEDs compared to the traditional LEDs are, easy to fabricate large area of the device, mechanically flexibility and low cost. Besides this, the emission of OLEDs is broader, and the quality of the white light is better. However, the efficiency and lifetime of OLEDs are much lower than those of the traditional LEDs. Therefore, the history of performance improvement is about the history of OLEDs development. The internal quantum efficiency (IQE) of OLEDs can be given:

$$\eta_{IQE} = \frac{number\ of\ photons}{number\ of\ electrons} = \eta_{e/h} \cdot \eta_{PL} \cdot \eta_{exci} \qquad (1.2),$$

where η_{IQE}, $\eta_{e/h}$, η_{PL}, and η_{exci} are the IQE, the charge balance factor, quantum yield, and fraction of excitons capable of radiative relaxation, respectively. Therefore, if we want to improve the efficiency performance of OLEDs, we need to improve the three product terms.

First, in other to improve the charge balance factor $\eta_{e/h}$, we need to optimize the structures of the OLEDs. The earliest observation of electroluminescence (EL) in organic semiconductor was in the 1950s by André Bernanose et al. [17-20] In the 1960s and 70s, the structure of the early OLEDs consists of a single layer OLED (shown in Figure 1.6). [21,22] In 1987, two employees, Ching W. Tang, and Steven Van Slyke, working at Eastman Kodak made the first practical OLED, which was a bilayer OLED (shown in Figure 1.7). [23] The bilayer structure balances the different mobilities of the electrons and holes in the organic semiconductor materials. It also lowers the injection barriers of the electrons and holes of the organic semiconductor materials. Based on the property of the excitons in the organic semiconductor, we could keep optimizing the bilayer structure (shown in Fig 1.8). [24] This structure prohibits the exciton from diffusing to the electrodes and extinguishing because it confines the exciton within the narrow-gap materials.

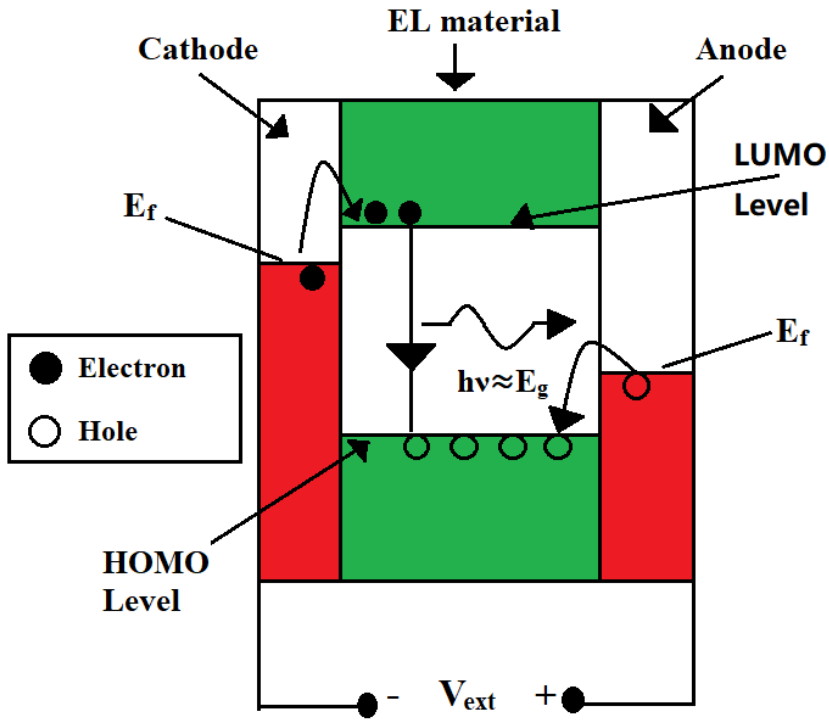

Figure 1.6 The structure of the single layer OLED, where HOMO level is the highest occupied molecular orbit and LUMO level is the lowest unoccupied molecular orbit.

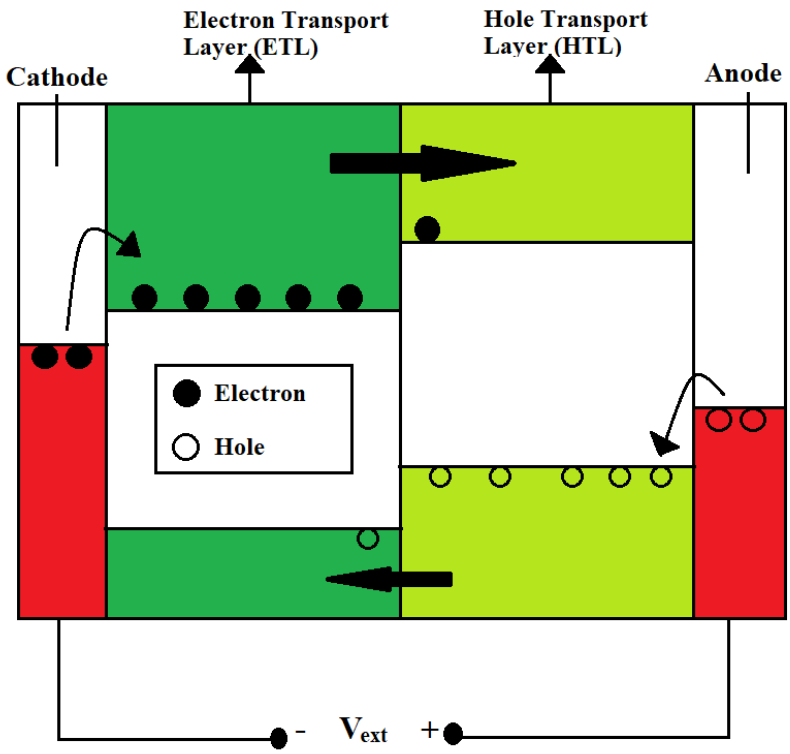

Figure 1.7 The structure of the bilayer OLED. One of the ETL and HTL is the electroluminescent layer.

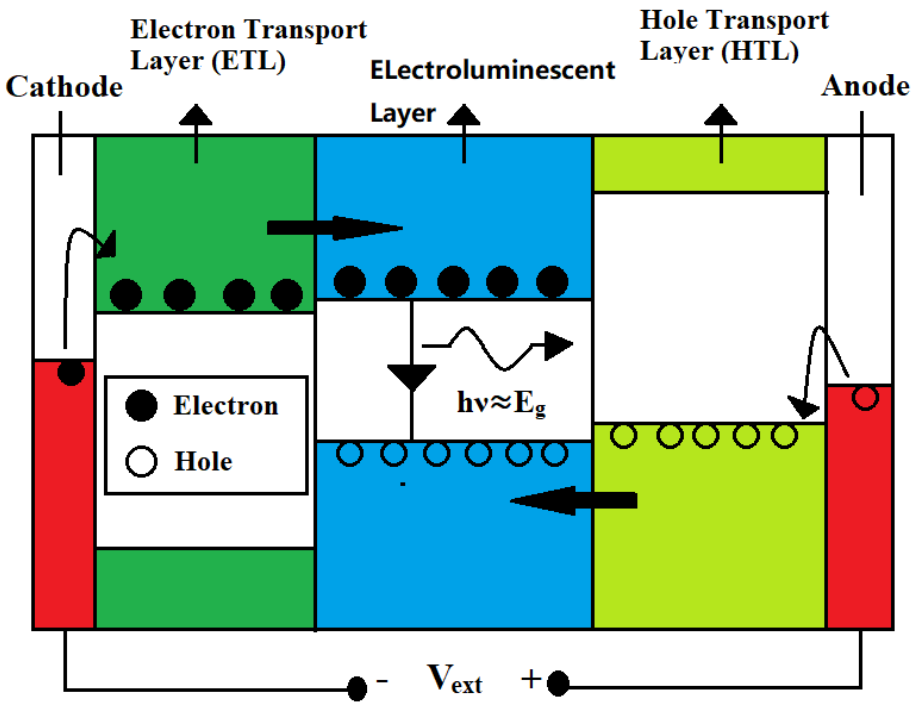

Figure 1.8 The structure of the optimized bilayer OLED. The energy gap of electroluminescent material is smaller than the energy gap of ETL or HTL.

Secondly, to improve the η_{PL} and η_{exci}, we need to optimize the emitters of the OLEDs. For every OLEDs, the injected electrons and holes form 25% singlets and 75% triplets (shown in Figure 1.9). Without the spin-orbital coupling, only the singlets can radiatively decay. Therefore, all first-generation OLEDs used fluorescent emitters (singlet emitters), [24] the IQE limit is 25%. To take advantage of the triplets, phosphorescent emitters (triplet emitters) were used. In the molecules of the triplet emitters, there must be some heavy metal atoms (shown in Figure 1.10) [25,26]. The orbital magnetic field produced by these larger atomic nuclei is stronger enough to invert the spin of the electron due to those interactions and allow the triplet-singlet transition to occur. This made the IQE limit of the second-generation OLEDs to achieve a 100%. However, the too long triplet decay time is a major disadvantage of the second-generation OLEDs. In addition to the radiative recombination, there are two electronic transitions for the triplet decay: triplet-triplet annihilation and triplet-polaron annihilation. The too long triplet lifetime increases the fraction of the annihilation and decreases the efficiency (efficiency roll-off). Therefore, to avoid this issue, researchers invented a third generation OLEDs. The third-generation OLEDs still uses the singlet emitters (delay fluorescent emitters). [27-29] The new mechanism called thermal activated delay fluorescence (TADF), could eliminate the efficiency roll-off issue (shown in Figure 1.11). Because the energy gap between singlet excited state S_1 and triplet excited state T_1 is very small, it is therefore easy to raise triplet-singlet electronic transition without heavy metal atoms. Although the blue OLEDs with TADF emitters have met a breakthrough on external quantum efficiency (EQE) in 2014 by Adachi et al., [28,29] the efficiency performance still has a lot of room to improve.

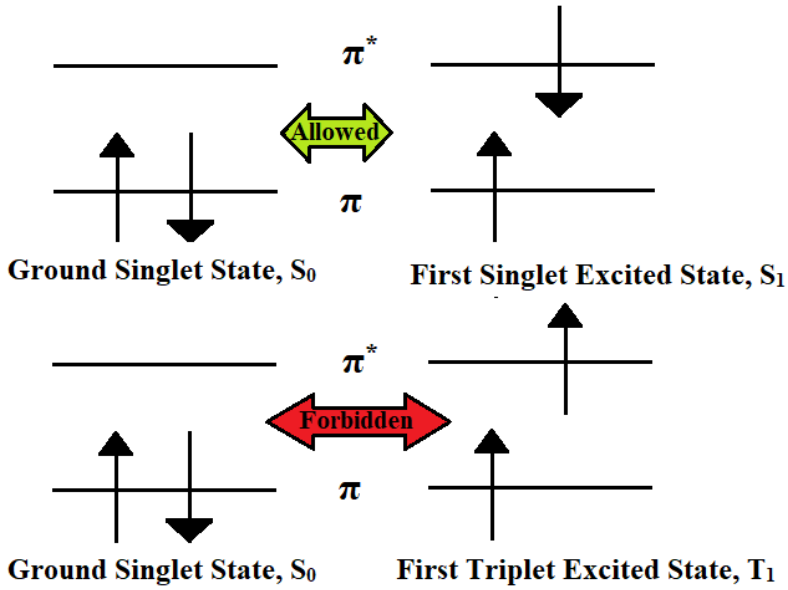

Figure 1.9 Diagram of the ground singlet state S0, first singlet excited state S1 and first triplet excited state. The π is the bonding molecular orbit and π* is the antibonding molecular orbit.

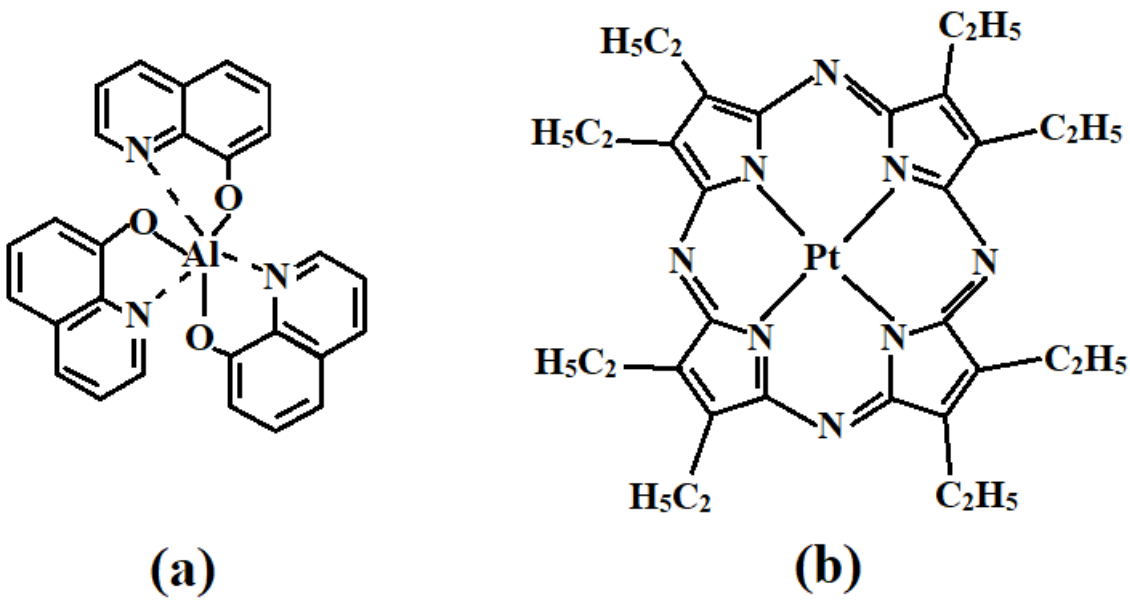

Figure 1.10 Two typical phosphorescent emitters from [25, 26].

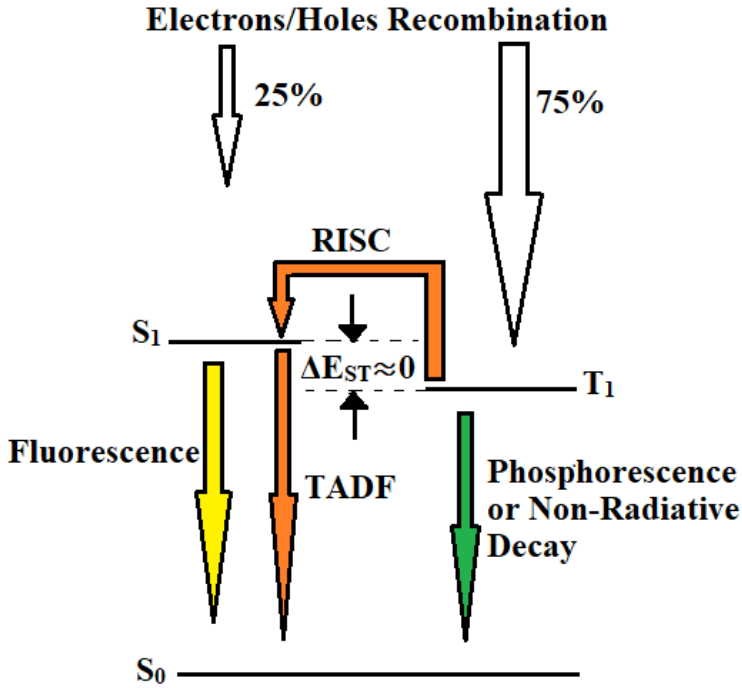

Figure 1.11 Diagram of TADF process. The requirement for TADF process is that the energy gap ΔEST between first singlet S1 and first triplet T1 should almost equal 0. This increases the possibilities of reverse intersystem crossing (RISC) process.

1.2.5 Micro-LEDs

Although OLEDs have been widely used on cellphone screens and other small displays, due to their intrinsic bad efficiency performance and short lifetime, most technology companies like Apple still think that OLEDs will not be the best choice of screens for the future. Presently, μ-LEDs displays are considered as the new generation displays. The μ-LEDs technology scales the LEDs we see today to lengths of tens of microns or even microns and integrates the RGB colors LEDs on the same substrate as a μ-display. Compared to the OLEDs displays and LCD, μ-LEDs displays have the highest luminance, fastest speed, and highest contrast. However, there are still some drawbacks to the μ-LEDs technology which should be tackled before they become widely used.

First, it is very difficult to integrate the RGB three colors LEDs on the same substrate. From section 1.2.2, we stated that different color LEDs need different luminescent semiconductor materials. One way to surmount this is by integrating the RGB three colors LEDs on Si substrates.

There are some technologies to transfer the GaAs based and GaN based LEDs onto a Si substrate, [30,31] but the costs are exorbitantly high. Another way is integrating RGB LEDs on the flexible substrate. This follows the development of the displays, but it may not possibly win the OLEDs due to the compatibility problems.

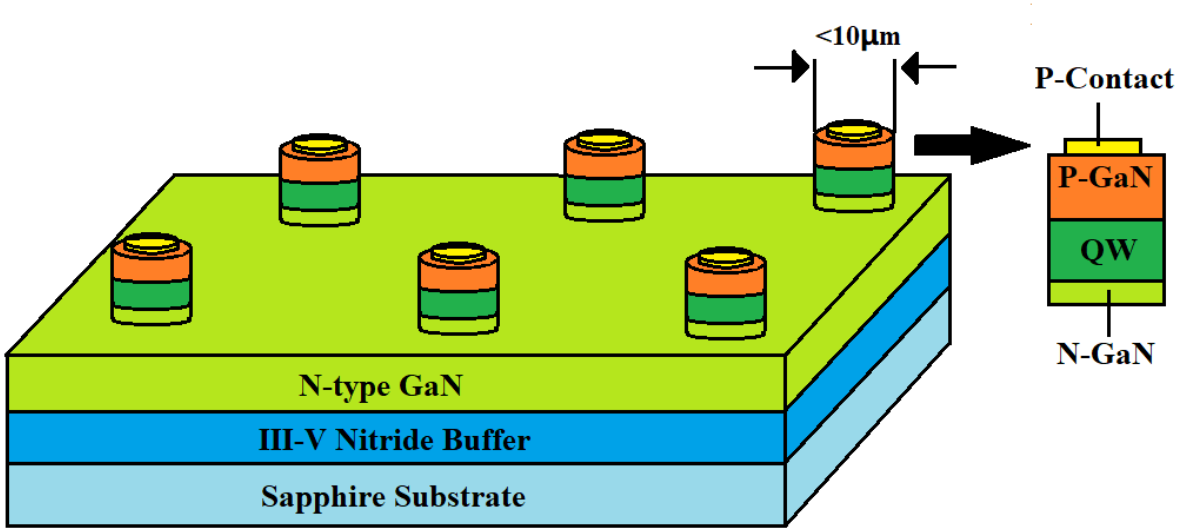

Figure 1.12 Structure of GaN/InGaN μ-LEDs in microns dimension. The GaN/InGaN μ-LEDs form an array by etching process from [32].

The other drawback with the μ-LEDs is the efficiency performance, which is due to the surface recombination effect. During the early 21st century, some researchers fabricated GaN-based μ-LEDs in microns dimension (shown in Figure 1.12), but the efficiency was lower than 1.5%. [32-36] The reason for the low efficiency is due to the high surface recombination of the μ-LEDs. With the development of new technology, present researchers have fabricated some better μ-LEDs structures to suppress the surface recombination. One fabrication method called side-wall passivation is shown in Figure 1.13. Dupré et al. [37] applied this method and successfully fabricated an 8μm μ-LED within 873 x 500 pixels matrix with 16% EQE. Another method is the long thermal annealing of the device after etching. Tian et al. [38] used this fabrication technology and successfully fabricated a 6μm μ-LED with 10% EQE. These two technologies have their advantages and disadvantages, and none of them could be used for mass production currently. Therefore, this thesis provides some new LED designs to suppress the surface recombination and improve the efficiency performance.

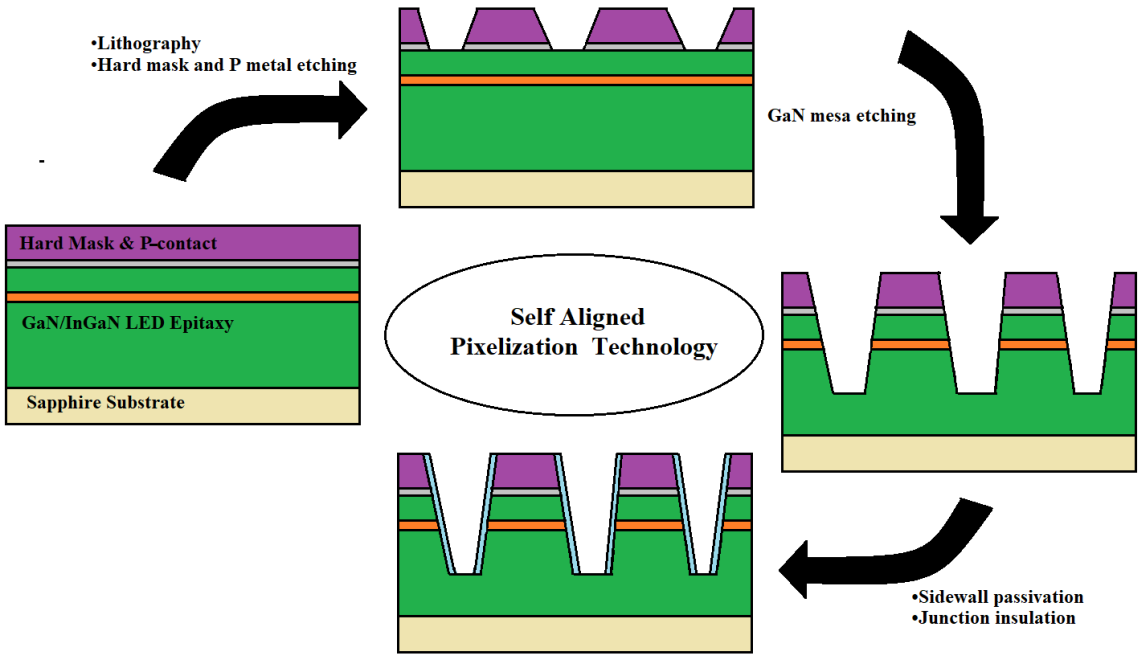

Figure 1.13 Steps of the sidewall passivation process from [37].

1.3 Research Objective

According to previous researches, quantum efficiency of GaN/InGaN significantly drops as size shrinks down. In this thesis, the research goal is to investigate the mechanism which dominates the size-dependent efficiency performance of GaN/InGaN μ-LEDs and find a way to effectively improve the quantum efficiency of GaN/InGaN μ-LEDs by analyzing the simulation and experimental results.

1.4 Thesis Overview

This thesis focuses on simulation and analysis of the GaN based μ-LEDs, especially smaller micron sizes (<10μm). Moreover, the new design is introduced to improve the efficiency performance of μ-LEDs in microns dimension.

Chapter 2 introduces the internal quantum efficiency model with different radiative processes, including the wanted radiative recombination, unwanted auger recombination, and Shockley-Read-Hall (SRH) recombination. The IQE model explains and summarized three main reasons to

which the efficiency droop problem at higher injected current density can be attributed when the GaN based LEDs are in bigger sizes. However, when the size shrinks down, the IQE model also explains that the high surface recombination, which arises due to different etching processes, can significantly decrease the efficiency of the GaN-based μ-LEDs. The simulated model is set up using Crosslight APSYS software, and the results show that by setting the surface recombination rate with reasonable parameters, the peak IQE value of μ-LEDs decreases from 53% to 4% when the size shrinks down from 100μm to 5μm.

Chapter 3 describes the temperature-dependent measured efficiency performance on 50×50 μm^2 GaN based μ-LEDs, and showed great agreement with the simulation results, proving the reliability of the simulation. The unusual efficiency performance of the GaN based LEDs at low temperature can be attributed to the property of Indium and the high ionized energy of GaN: Mg.

Chapter 4 introduces a new LED design with n-doped quantum barriers in the active region. According to previous research, the GaN-based LED with p-doped quantum barriers is a common strategy to relieve the efficiency droop problem by balancing the hole and electron concentration. However, when the size of GaN-based μ-LEDs shrinks down, this strategy becomes invalid. But with the GaN-based μ-LED with n-doped quantum barriers, the shrinking causes the IQE to increase. The reason is that the SRH recombination rate (surface recombination) in n-GaN is much smaller than in p-GaN. Under the tradeoff between electron-hole injection balance and non-radiative SRH recombination, the 5×5 μm^2 GaN-based μ-LEDs with n-doped quantum barrier and optimal doping concentration exhibit more than 100% efficiency improvement at 20$A \cdot cm^{-1}$ compared to a conventional intrinsic multiple quantum wells (MQWs) based design.

In summary, a comprehensive study of GaN based μ-LEDs, which entails the theoretical principles, model derivation, reliable simulation, analysis of test results and innovative construction, is reported in this thesis. Besides, this thesis also exhibits how surface recombination impacts on the efficiency performance of size-dependent GaN based μ-LEDs. The new LED structures proposed in this study can suppress the surface recombination and significantly improve the efficiency of the 5×5 μm^2 GaN based μ-LEDs.

Chapter 2 Impact of Different Recombination on Efficiency Performance of Size-Dependent GaN/InGaN μ-LEDs

2.1 Internal Quantum Efficiency Model of GaN/InGaN LEDs with different carrier recombination mechanisms

2.1.1 Radiative Recombination

In semiconductors, carrier generation and recombination are the most common processes to generate or eliminate free carriers, including electrons and holes. As shown in Figure 2.1, almost all the solids have similar electronic band structures which include conduction band, band gap and valence band structures, respectively. The bands below the valence band (including valence band) are almost filled and the bands above the conduction band (including conduction band) are almost empty. Only electrons in bands above the conduction bands can freely move and contribute to the electric current. Therefore, the phenomenon where electrons in the bands below the valence bands receive energy by heat-up or electric field and reach the conduction band is called carrier generation. The reverse process is called carrier recombination.

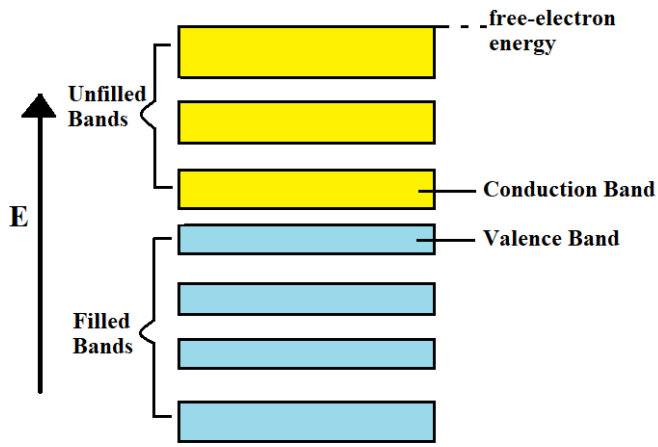

Figure 2.1 The electronic band structure of solid materials.

Normally, the carrier generation and recombination processes can be classified based on the interaction with photons, phonons, other electrons or other holes during the processes. Therefore, the carrier generation and recombination processes involving photons are called photon absorption and radiative recombination. The wavelength of the emitted photon is determined by the bandgap energy of the semiconductor materials. In LED, this recombination process is what we need. Therefore, by using heterojunction QW structures and semiconductor materials with direct band gaps (shown in Figure 2.2), the radiative recombination process can play a major role in LEDs.

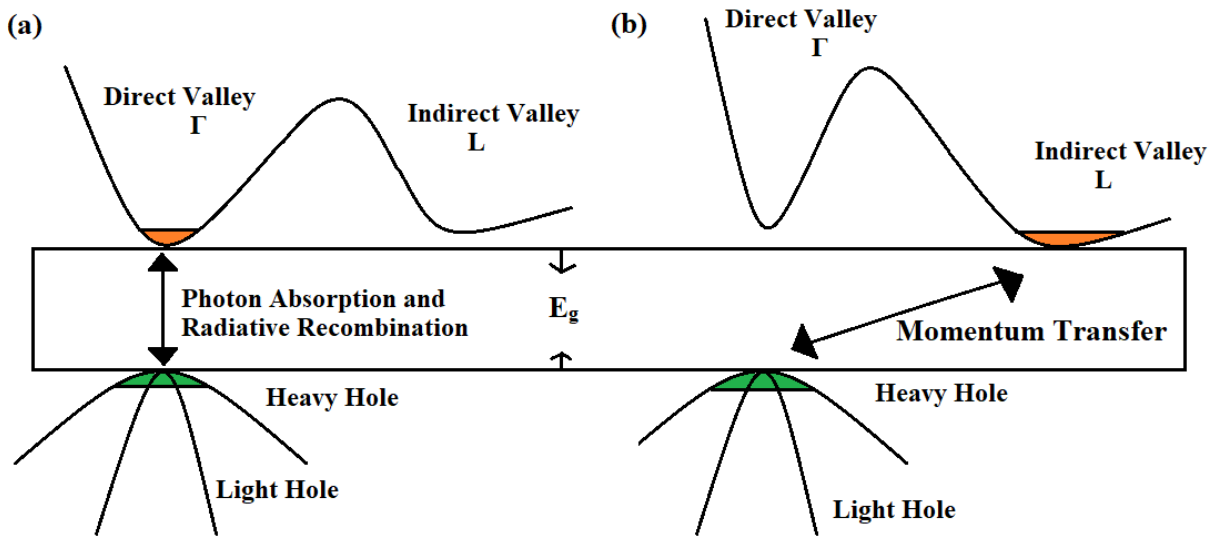

Figure 2.2 Diagram of (a) direct bandgap and (b) indirect bandgap of a semiconductor.

The radiative recombination rate R_{rad} is calculated by:

$$R_{rad} = \mathrm{Bnp},\ ^{[39]} \tag{2.1}$$

Where n and p are the concentrations of free electrons and holes and B is a constant so-called radiative capture probability or radiative coefficient for a given semiconductor.

2.1.2 Auger Recombination

The carrier generation and recombination processes involving high energy electrons are called impact ionization effect and Auger recombination (Auger effect). In the impact ionization effect, some high energy electrons collide with atoms in the semiconductor materials and transfer energy to the electrons in lower energy orbitals. These newly excited electrons jump to the higher energy orbitals and create electron/hole pairs. On the other hand, in Auger recombination (shown in Figure 2.3), instead of emitting photons, the released energy from electron/hole pairs recombination is transferred to some second electrons. The excited electrons collide with atoms of the semiconductor materials and relax back in the low energy orbitals. The Auger recombination

process also occurs with excited or high energy holes, which depends on or involved free carriers. Because the Auger recombination requires energy exchange between carriers, the probability of this process increases when the carrier density increases. The Auger recombination R_A rate can be given by:

$$R_A = C_n n^2 p + C_p p^2 n, (4)\ [39] \tag{2.2}$$

Where C_n *and* C_p are constants called Auger capture probabilities or Auger coefficients for a given semiconductor.

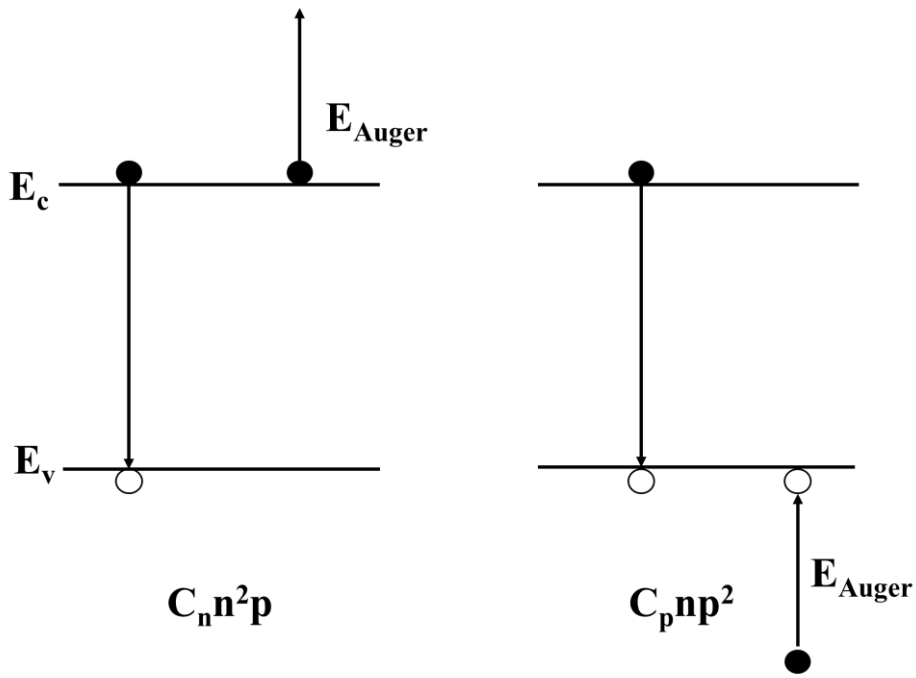

Figure 2.3 The views of the Auger effect.

2.1.3 Shockley-Read-Hall Recombination

Both the radiative recombination and the Auger recombination are a band to band one-step recombination processes. There is another two-step recombination process named SRH recombination (shown in Figure 2.4). This recombination process occurs due to the presence of defects in the semiconductor materials. The crystal defects or impurities modify the band structures and introduce trap levels in the forbidden band between the conduction band and valence band. The free electrons in the conduction band can relax back and be trapped in the trap levels. After a short period, the electrons in the trap levels relax back to the valence band with emission of photons or phonons. The SRH recombination rate can be given by [40]

$$R_{SRH} = \frac{np - n_i^2}{\tau_p(n+n_1)+\tau_n(p+p_1)}, \tag{2.3}$$

Where n_i is the intrinsic carrier concentration of the given materials, τ_p and τ_n are the recombination lifetime for holes and electrons respectively. The parameters n_1 and p_1 depend on the trap level E_t and are given by

$$n_1 = N_c \exp\left(\frac{-E_c+E_t}{kT}\right), \tag{2.4}$$

$$p_1 = N_v \exp\left(\frac{-E_t+E_v}{kT}\right), \tag{2.5}$$

Where N_c and N_v are the carrier effective density of states for electrons and holes respectively, k is the Boltzmann constant and T is the temperature.

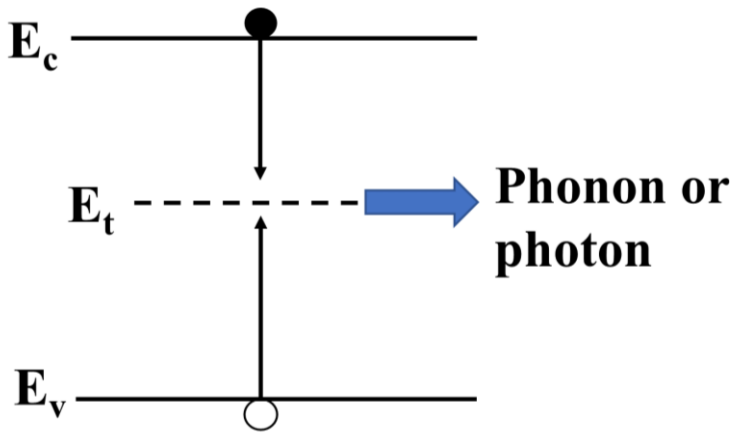

Figure 2.4 The view of SRH recombination (trap-assisted recombination), Et is the energy level of the traps.

2.1.4 Internal Quantum Efficiency Model

Normally, the EQE of LED is a product of two parts: the IQE and the extraction efficiency (η_c). Generally, the extraction efficiency can be considered as a constant when the injection current changes. Moreover, in μ-LEDs, the extraction efficiency which accounts for the photon lost is close to 1 due to the small volumes of μ-LEDs. Therefore, we considered the IQE as the key parameter to address the efficiency droop problem.

As mentioned above, the injected electrons and holes can have three types of recombination in the QWs or outside of the QWs. Therefore, we can define η_{IQE} as a fraction of the injected current which can generate photon:

$$\eta_{IQE} = \frac{I_{rad}}{I_{total}}. \tag{2.6}$$

The total injected current I_{total} can be divided into 4 parts, I_{rad}, I_{Auger}, I_{SRH} and I_{leak} (shown in Figure

2.5). The leakage current I_{leak} includes all the recombination process outside the QWs and we can define the injection efficiency η_{inj} as

$$\eta_{inj} = \frac{I_{toal} - I_{leak}}{I_{total}}, \tag{2.7}$$

and the Eq. 2.7 can transform to

$$\eta_{IQE} = \frac{\eta_{inj} I_{rad}}{I_{rad} + I_{SRH} + I_{Auger}}. \tag{2.8}$$

To more simplify Eq. 2.8, the simple ABC model is introduced as [41]

$$\eta_{IQE} = \frac{\eta_{inj} BN^2}{AN + BN^2 + CN^3}. \tag{2.9}$$

The ABC model in Eq. 2.9 is based on Eq. 2.1, 2.2 and 2.3, where N is the carrier density in QWs and A, B, C are the SRH recombination coefficient, the radiative coefficient, and the Auger coefficient, respectively. With the ABC model researchers can now analyze the initial reasons for the efficiency droop in GaN-based μ-LEDs.

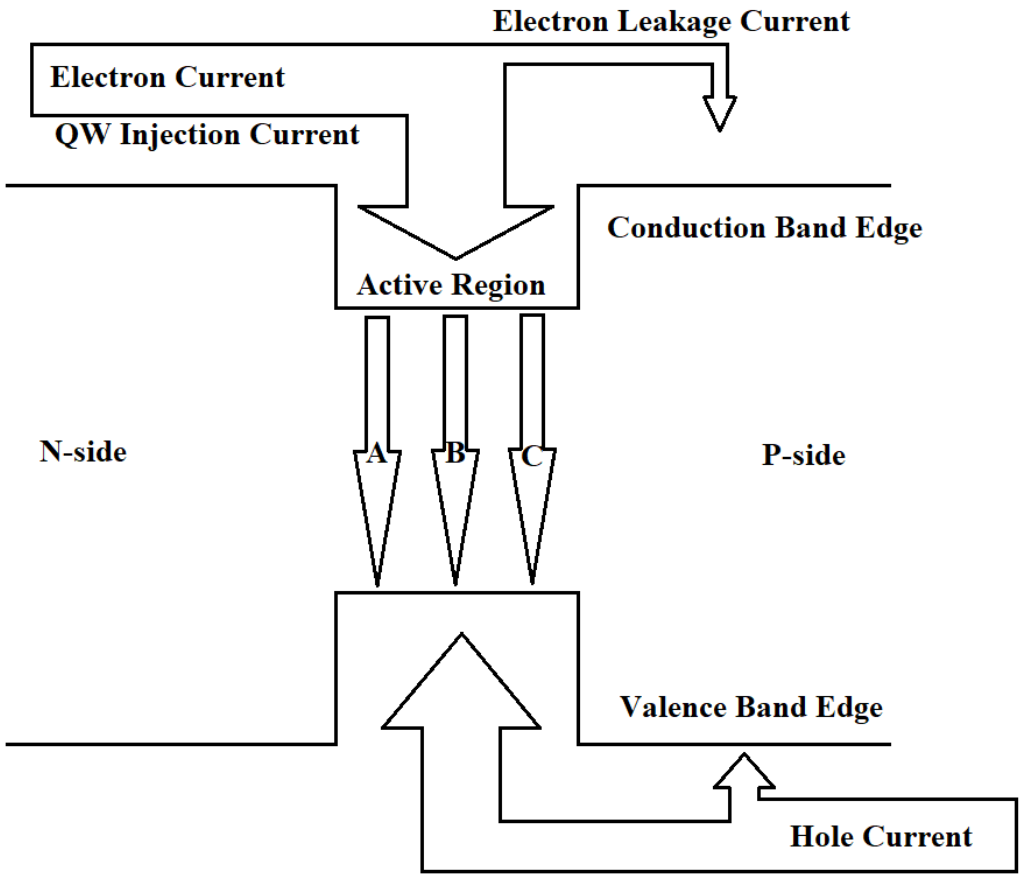

Figure 2.5 View of the total current from [41], where A, B, C are the current for SRH recombination, radiative recombination, and Auger recombination, respectively.

2.2 Major Mechanisms of Efficiency Droop Phenomenon in GaN/InGaN LEDs

As a solid-state lighting source with high luminance and long life-time, the gallium nitride (GaN)/indium gallium nitride (InGaN) micro light-emitting diodes (μ-LEDs) is considered a promising technology for many applications, including as light source for optogenetic neuron stimulation, [42,43] micro-indicators [44] and self-emissive micro-displays. [45,46] However, since blue LEDs are required for making any kind of white LEDs, the GaN/InGaN LEDs can be considered the most important LEDs compared to all other material-based LEDs. Although blue GaN/InGaN LEDs have made some significant progress, there are still some problems which should be addressed. The biggest challenge with the GaN/InGaN LEDs is so-called efficiency droop. It describes a phenomenon in which the IQE (EQE) decreases gradually as the injected current increase. The efficiency droop phenomenon has been attributed to three main cause: Auger recombination, low hole injection and carrier overflow.

2.2.1 Efficiency Droop in GaN/InGaN LEDs: Auger Effect

As we mentioned in section 2.1.2, the probability of Auger recombination increases when the carrier density increases. At low injection current level, the Auger recombination process can usually be ignored; but at high injection current level, Auger recombination starts to dominate the recombination processes. Therefore, we can simplify Eq. 2.9 into

$$\eta_{IQE} = \frac{\eta_{inj} B}{CN}. \tag{2.10}$$

According to Eq. 2.10, we see that considering η_{inj}, B and C as constants, η_{IQE} and N (injected current) are inversely proportional. In 2013, Iveland et al. [47] claimed that they have proven that Auger recombination is the dominant mechanism for efficiency droop by a direct measurement. They collected high energetic electrons generated by Auger recombination emitted from the QW regions with the Faraday cup (shown in Figure 2.6). The presence of the Auger electrons is exhibited by high energy peaks in the electron energy distribution curves. The authors discovered that the Auger electron current peaks are simultaneously well correlated with the observed efficiency droop. This measured results indeed confirmed that Auger recombination process induces the efficiency droop phenomenon in GaN/InGaN LEDs, but it cannot prove whether Auger recombination is the only cause.

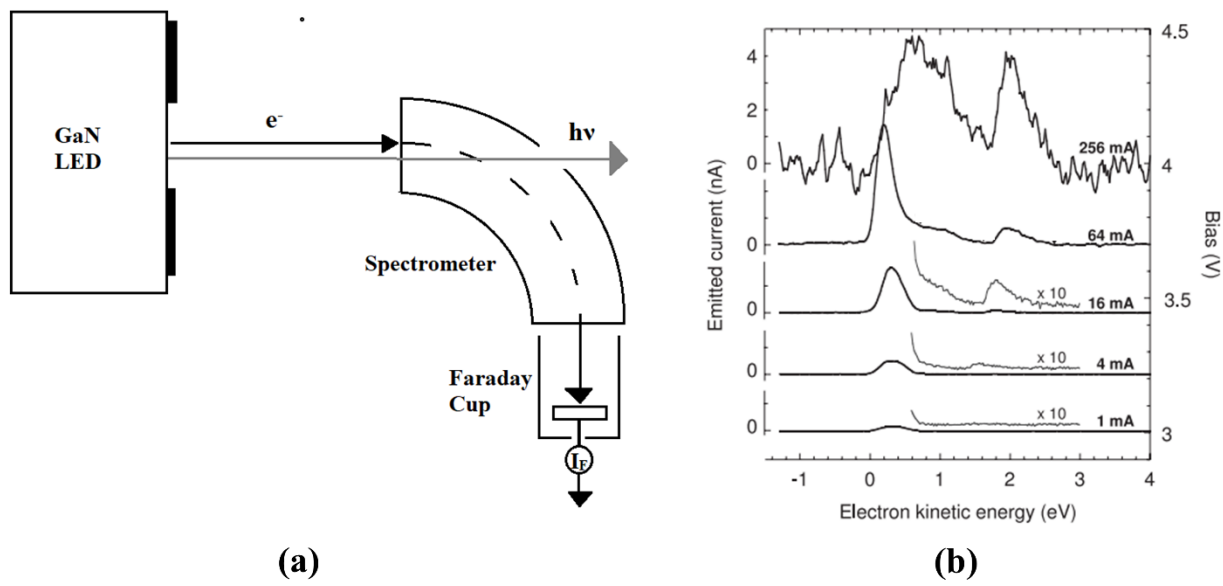

Figure 2.6 (a) The experiment to collect high energetic electrons generated by Auger recombination emitted from the QW regions with the Faraday cup in [47]; (b) the energy distribution curves for different injection currents from [47]. When current increases, high energy peaks which appear around 2 eV represent the generation of hot carriers by Auger effect.

2.2.2 Efficiency Droop in GaN/InGaN LEDs: Carrier Overflow

Although heterojunction QW structure is a very efficient structure to harvest injected current that recombines in selected semiconductor materials, a portion of the injected carriers still bypass the QW structure. The built-in electronic polarization in GaN/InGaN LEDs due to the absence of centrosymmetry in the wurtzite crystal structure aggravates the carrier overflow problem. [48] The built-in electric field F is obtained by Gauss's law:

$$F = \frac{q\sigma_s}{\varepsilon_s}, \tag{2.11}$$

Where q is the elementary charge, σ_s is the sheet density of fixed sheet charge at heterojunction and ε_s is the semiconductor dielectric constant. The IQE of GaN/InGaN LEDs are very sensitive to the built-in electric field F due to the quantum-confined Stark effect. The internal polarization field and the junction field of state-of-art GaN/InGaN LEDs which grow on an n-type Ga-polar c-plane GaN substrate have inverse directions (shown in Figure 2.7). When the forward-bias current injects into the LEDs, the electrons are accelerated by the built-in electric field and overflow the

QW regions. Our rough calculation estimates that half of the efficiency droop is due to the polarization electric field.

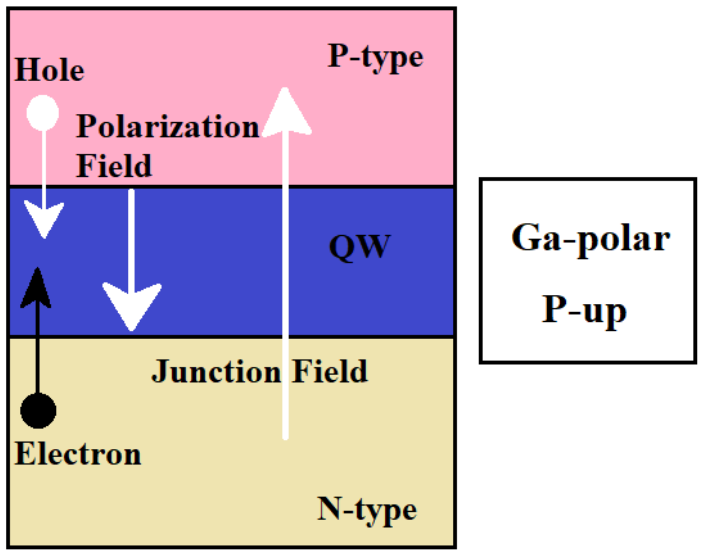

Figure 2.7 The view showing the direction of the polarization field and junction field in GaN/InGaN LED. [50]

To control the polarization effect, the researchers have added an extra AlGaN layer in-between the p-type regions and QW regions, which is called the electron blocking layer (EBL). [49] This layer with appropriate Al composition can block the electrons which overflow through the QW regions and improve the efficiency performance of the GaN/InGaN LEDs. The P-I-N LED structure with EBL is the standard LED structure which we currently use. This year, Dr. Turski with his teammates proposed that GaN/InGaN LEDs with bottom tunnel junction can control the polarization effect and improve the efficiency performance of GaN/InGaN LEDs at high injection current density. [50] The bottom tunnel junction structure (shown in Figure 2.8) can make the polarization electric field and junction field with the same direction but keep the high-quality n-type GaN substrate. The injected electrons in the forward-bias current are slowed down by the polarization electric field which eliminates the carrier overflow problem.

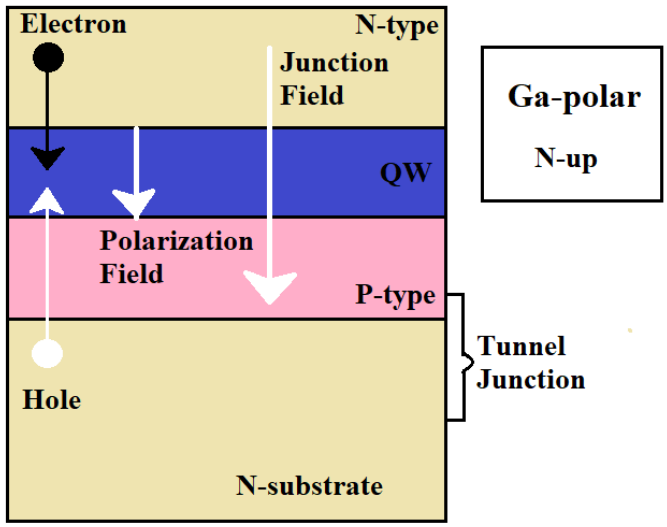

Figure 2.8 The structure of GaN/InGaN LEDs with bottom tunnel junction structure. [50]

2.2.3 Efficiency Droop in GaN/InGaN LEDs: Hole Transportation Problem

GaN/InGaN LEDs are bipolar devices and require both holes and electrons to be effectively injected and uniformly distributed in the QWs active regions. Therefore, a high-efficiency GaN/InGaN LEDs prefer balanced holes and electrons distribution in the QWs. However, the mobilities of the holes and electrons in GaN/InGaN have a large difference. The maximum electron mobility $\mu_{max,e}$ in GaN is around 1000 $cm^2V^{-1}s^{-1}$ while the maximum hole mobility $\mu_{max,h}$ in GaN is around 170 $cm^2V^{-1}s^{-1}$. [51] Following the carrier density increase, the electron and hole mobility decreases and got close to the minimum value. The minimum electron mobility $\mu_{min,e}$ in GaN is around 55 $cm^2V^{-1}s^{-1}$ and the minimum hole mobility $\mu_{min,h}$ in GaN is around 3 $cm^2V^{-1}s^{-1}$. Therefore, the recombination center where the doping concentration of electrons can balance the doping concentration of holes would be near the p-type layer. This phenomenon reduces the efficiency performance and would be more serious when the injected current increase.

There are some methods to improve hole transport in GaN/InGaN LEDs. One of the popular methods is p-doped quantum barriers. [52] The p-doped quantum barriers increase the injection efficiency of holes in the QWs active region. Adjusting the barriers thickness or the EBL thickness can also improve the hole transport. [53] However, due to the large difference between the hole and electron mobilities, the imbalance between electrons and holes in GaN cannot be fully eliminated without the introduction of other materials.

2.2.4 Efficiency Droop in GaN/InGaN μ-LEDs: Surface Recombination

To show how surface recombination affects the IQE, we initially began with a derivation of Eq. 2.9, the IQE ABC model. To indicate that η_{IQE} is a function of carrier density N, we calculated the maximum value of η_{IQE} by computing the derivate of Eq. 2.9. When $d\eta_{IQE}/dN = 0$, η_{IQE} reaches the maximum value. Therefore, we deduced that the peak position of carrier density is given by

$$N_{peak} = \sqrt{A/C}, \tag{2.12}$$

and the maximum value of η_{IQE} is given as

$$\eta_{IQE,max} = \frac{\eta_{inj} B\sqrt{A}}{2A\sqrt{C}+B\sqrt{A}}. \tag{2.13}$$

According to Eq. 2.13, we can see that if SRH recombination coefficient A increases, the maximum value of η_{IQE} decreases. Previous researchers show that, although there are a large number of threading dislocations (TDs) in the InGaN active regions, the IQE of GaN/InGaN LEDs is higher than every other III-V compound semiconductor-based LEDs. [54] Also compared to other III-V compound semiconductor-based LEDs, the GaN/InGaN LEDs are less sensitive to the bulk defects.

Besides, the surface recombination which is also a kind of SRH recombination can usually be ignored in GaN/InGaN LEDs. Also observed is that almost all the etching procedure, such as plasma etch for defining the shape of micro-LED mesas or wet etching, will severely disrupt the crystal lattice and produce surface recombination defects. Recombination defects near the surface will deplete the carriers in this region and draw carriers from the surrounding regions, resulting in lateral leakage current and drastic efficiency drop. The most important parameter which is the surface recombination velocity (SRV) reflects the impact of the surface recombination on efficiency. SRV describes how fast the carriers drift toward the recombination surface. The other related parameter to the SRV is the diffusion length of the electrons and holes. Both parameters play important roles in determining the device efficiency. The SRV in GaN is typically around 1×10^2 cm/s to 1×10^5 cm/s. [55] The reason that the surface recombination in GaN/InGaN LEDs can be ignored is that the SRV in GaN and InGaN is much smaller than those of other III-V compound semiconductors. However, when the size of μ-LEDs shrinks down to a few micrometers, the efficiency performance of GaN/InGaN μ-LEDs suffers a high surface recombination rate. [56-58]

The reason that the surface recombination plays a key role in the efficiency performance of micro-level μ-LEDs is due to the high surface area to volume ratio. Normally, to calculate the leakage current due to the surface recombination on the side-wall, only the lateral current was counted. Therefore, only the side-walls surface area to volume ratio was calculated. For a GaN/InGaN LED

with 100μm×100μm×2μm mesa, the side-wall surface area to volume ratio equals 0.04. However, for a GaN/InGaN μ-LED with 5μm×5μm×2μm mesa, the side wall surface area to volume ratio equals 0.8. That is 20 times higher than the former LED. With a similar surface defect density, the SRH recombination coefficient should be 20 times higher as well.

The surface recombination rate is given by:

$$R_s = \frac{np - n_i^2}{p + n + 2n_i \cosh\left(\frac{E_i - E_{st}}{kT}\right)} N_{st} v_{th} \sigma, \tag{2.14}$$

where p and n are the hole and electron concentrations at the surface region, E_{st} is the energy level of the surface defect, N_{st} is the density of the surface defect, v_{th} is the thermal velocity, and σ is the capture cross-section of the surface defect. The parameter SRV v_s is given by:

$$v_s = N_{st} v_{th} \sigma. \tag{2.15}$$

The Eq. 2.14 is almost identical to the Eq. 2.3, the SRH recombination rate expression. The only difference is that the parameter N_{st} in Eq. 2.14 is a 2D parameter. To easily evaluate a reasonable value of SRV, a simple equation is given as: [59,60]

$$v_s = A' \times D, \tag{2.16}$$

where A' is the SRH surface recombination coefficient and D is the diameter of the device mesa. The reasonable parameter A' for a top-down etched μ-LED without the use of expensive sidewall passivation treatment can be found in reference [61]. The calculated SRV at room temperature (300 K) is between 2×10^4 cm/s to 3×10^4 cm/s. Here, we set the SRV as 3×10^4 cm/s at room temperature and the simulation tool APSYS is employed to simulate GaN/InGaN μ-LEDs.

2.3 3D Modeling of GaN/InGaN LEDs in Crosslight APSYS

APSYS, Advanced Physical Models of Semiconductor Devices, is based on the 2D/3D finite element analysis of the electrical, optical and thermal properties of modern semiconductor devices. [62] To simulate the MQW GaN/InGaN LEDs, some models in APSYS are used. The most important ones are the drift-diffusion model and self-consistent MQW model. The running steps to construct the LED structure and to finish the simulation are also given in chapter 2.3.3.

2.3.1 Drift-Diffusion Model in Semiconductor

The Poisson's equation is the basic equation to describe the behavior of semiconductor device:

$$\nabla \cdot \nabla \phi = -\frac{q}{\varepsilon}(p - n + N_D^+ - N_A^- + \rho_p - \rho_n), \tag{2.16}$$

Where Φ is the electrostatic potential; N_D^+ and N_A^- are the ionized donors and acceptors; ρ_p and ρ_n are the fixed charge from traps. The other basic equations are the current continuity equations for the electrons and holes:

$$\nabla \cdot \frac{J_n}{q} = \frac{\partial n}{\partial t} - \frac{\partial N_D^+}{\partial t} + \frac{\partial \rho_n}{\partial t} + R, \tag{2.17}$$

$$\nabla \cdot \frac{J_p}{q} = \frac{\partial N_A^-}{\partial t} - \frac{\partial p}{\partial t} - \frac{\partial \rho_p}{\partial t} - R, \tag{2.18}$$

Where J_n and J_p are the electron and hole current density; R is the recombination rate for electrons and holes including all the recombination types mentioned earlier in this work.

Int chapter 3, we will check the reliability of the simulation result by measuring the temperature-dependent performance of GaN/InGaN μ-LEDs. For the accuracy of the simulated temperature-dependent performance, incomplete ionization of the dopants model is also used in the simulation. The possibilities of occupancy for electron and hole shallow traps (dopants), which describes the degree of incomplete ionization, are given by: [59]

$$f_D = \frac{1}{1 + g_d^{-1} \exp\left(\frac{E_D - E_{fn}}{kT}\right)}, \tag{2.19}$$

$$f_A = \frac{1}{1 + g_a^{-1} \exp\left(\frac{E_A - E_{fp}}{kT}\right)}, \tag{2.20}$$

where E_{fn} and E_{fp} are the quasi-Fermi level of electrons and holes; E_D and E_A are the energy level of the shallow donors and acceptors; degeneracy levels g_d and g_a are automatically set to 2 and 4.

2.3.2 Self-Consistent MQW Model in GaN/InGaN LEDs

MQW models are one of the most complex models used in APSYS. To reach the accurate density

profiles and potential distribution in MQW structure, there are a few steps required to finish the calculation.

Firstly, we assumed that the MQW structure in LEDs is a flat-band condition at equilibrium. We also confined the carrier density within the well. The local electron density n is given as [59]

$$\mathrm{n}(x,y,z) = \frac{1}{d_w}\sum_j \rho_j^0 kT \ln\left[1 + exp\left[\frac{E_{f_n}(x,y,z) - E_j(x,y,z)}{kT}\right]\right], \quad inside\ the\ well$$
$$= 0, \quad \text{outside the well} \tag{2.21}$$

where E_j is the confined energy level in QWs; d_w is the thickness of QWs; ρ_j^0 is the density of the states of QWs. Eq. 2.21 gives the initial density profiles and potential distribution.

Secondly, still at equilibrium, we use the self-consistent model with the calculated potential from the first step. The electron density n in the self-consistent model is given as [59]

$$\mathrm{n(x,y,z)} = \sum_j g_n^j(y,z)\rho_j^0 kT ln\left[1 + \exp\left[\frac{E_{f_n}(x,y,z) - E_j}{kT}\right]\right], \tag{2.22}$$

Where we assumed that the QW is parallel to the x-axis and $g_n^j(y,z)$ is the electron wave function. The electron wave function and confined energy level E_j are obtained from the previous calculation at different bias. Eq. 2.22 gives the new density profiles and potential distribution.

Thirdly, by iterating the second step, the self-consistent numerical results of the density profiles and potential distribution are finally achieved. Once we achieved the self-consistent results, we increased the voltage bias and repeated the three steps above. By repeating these three steps hundreds or thousands of times, we finally obtained the simulation results.

2.3.3 Running Steps for APSYS

1. We constructed the "*.layer" file by setting detailed different information layers in the growth direction.
2. We run the "*.layer" to generate the "*.geo" files and run the "*.geo" to generate the mesh file.
3. We run the manual designed "*.sol" file by main equation solver and obtained the simulation results.

2.4 Simulated Results of GaN/InGaN μ-LEDs with Different Sizes

2.4.1 Simulated LED Structures and Parameters

To investigate the impact of surface recombination on the efficiency of size-dependent GaN/InGaN based μ-LEDs, simulations for the LED structures described below were carried out with APSYS modeling software. To simulate the IQE and EQE of GaN/InGaN μ-LEDs, we select few square-shaped devices with varying edge sizes of 5, 10, 50, and 100 μm. The LED structure is shown in Figure 2.9. The GaN/InGaN MQWs LEDs are grown on (0001) sapphire substrates with emission wavelength of 440 nm. The bottom layer of this device is made of 0.5-μm-thick n-type GaN with Silicon doping concentration of 1×10^{18} cm^{-3} and the top p-type GaN layer is made of 0.2-μm-thick layer with Mg-doping concentration of 1×10^{18} cm^{-3}. The QWs in the active region include 6 pairs of undoped 3-nm-thick $In_{0.18}Ga_{0.82}N$ QW layers with 40-nm-thick undoped GaN barriers in the middle of the QWs. Between the active region and the p-type GaN layer, a Mg-doped $Al_{0.15}Ga_{0.85}N$ layer is deposited as an EBL. The Ti/Au metal layers are sputter coated as a p- or n-ohmic contacts. The parameters used in this simulation work and their dependency on device operating temperature are summarized in Table 2.1 which includes SRV, screening coefficient of polarization effect *s*, [62] radiative recombination coefficient *B*, [41] bulk SRH lifetime τ_n and τ_p, [80,81] and Auger coefficient *C*. [82] The electron and hole mobility values are highly dependent on the carrier density and device temperature which can be found in technical manual of APSYS. [62] After a few errors and trials, we set the value of most important parameter SRV as 3×10^4 cm/s for our simulation work, because it reasonably agrees with our experimental data for a 50×50 μm^2 μ-LED.

Name	Value (at room temperature)	Temperature dependency
B	1×10^{-11} cm^3 s^{-1}	$B\propto T^{-1}$
τ_n	46 ps	$\tau\propto T^{-0.5}$
τ_p	12 ns	$\tau\propto T^{-0.5}$
C	10^{-34} cm^6 s^{-1}	$C\propto T^{0.5}$
s	0.5	Independent
SRV	3×10^4 cm s^{-1}	$SRV\propto T^{0.5}$

Table 2.1 The list of parameters and their corresponding values used in simulation along with their dependency on temperature. All these values are related to room temperature.

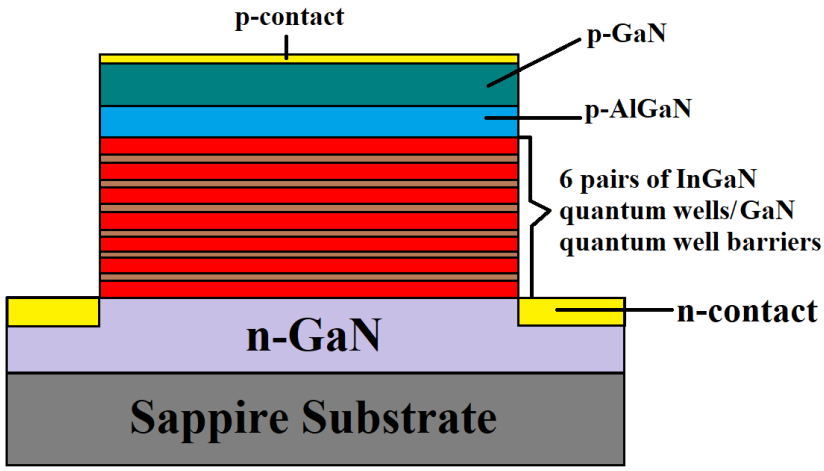

Figure 2.9 Structure of the simulated GaN/InGaN μ-LEDs.

2.4.2 Size-dependent Efficiency Performance

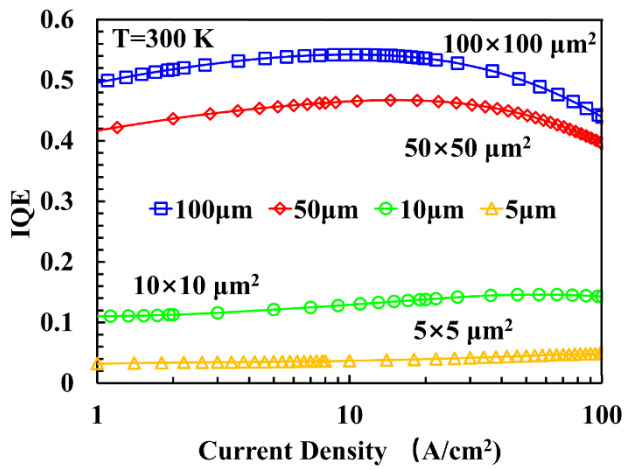

Figure 2.10 IQE as a function of current density (in log scale) curves of 4 different size μ-LEDs at room temperature.

Figure 2.10 shows the simulation results of the size-dependent efficiency performance of GaN/InGaN μ-LEDs at room temperature. The simulation results clearly showed that the IQE value significantly decreases as the device size shrinks, e. g., the peak IQE values drop from 54% for the 100×100 μm^2 and 47% for the 50×50 μm^2, 15% for the 10×10 μm^2 and around 5% for the 5×5 μm^2. This simulation results proved that the impact of surface recombination increases when the size decreases. Observation from Figure 2.10 indicates that as the size shrinks down, the peak positions of the IQE curves shift to the higher current density, e. g., the peak IQE positions shifted from around 10 $A \cdot cm^{-2}$ for the 100×100 μm^2 and 15 $A \cdot cm^{-2}$ for the 50×50 μm^2, 56 $A \cdot cm^{-2}$ for the

10×10 μm^2 and larger than 100 A•cm^{-2} for the 5×5 μm^2. This can be explained by Eq. 2.12. As mentioned earlier, the impact of surface recombination increases as the size shrinks down, which also means the SRH recombination coefficient A increases. If we assume the Auger coefficient C as a constant, the peak position $N=(A/C)^{0.5}$ increases following the increase in A. That is why the peak position shifted towards the higher current density. This also indicates that efficiency droop at higher injection current density is no longer accounts for the reduction of the efficiency performance of GaN/InGaN μ-LEDs when the size shrinks down to 5×5 μm^2. The new factor accounting for the efficiency droop of the micron size GaN/InGaN μ-LEDs at higher injection current density is the low maximum value of the IQE limited by the high surface recombination rate.

2.4.3 Size-dependent J-V Characteristic

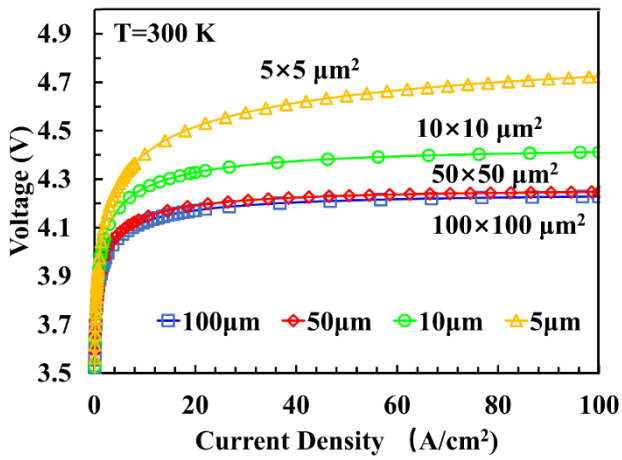

Figure 2.11 J-V curve of 4 different size μ-LEDs at room temperature.

Figure 2.11 shows four curves of GaN/InGaN μ-LEDs with different sizes at room temperature. The simulation results show that the driven voltage increases at the same current density when the size shrinks down. This phenomenon is also attributed to the high surface recombination in small size GaN/InGaN μ-LEDs. The high-density surface defects drift the free electrons and holes, thus, reduces the mean free path of electrons and holes in the injected current direction and increasing the resistivity of the device. Figure 2.11 shows the ideal IV curve of the devices with uniform current spreading. In reality, the ununiform current spreading of the devices with larger size results in higher resistance and larger voltage bias.

2.5 Conclusion

In this chapter, the impact of surface recombination on the efficiency of size-dependent GaN/InGaN μ-LEDs is investigated. The IQE model is introduced to analyze the mechanism that can affect the efficiency of GaN/InGaN μ-LEDs. Except for the Auger recombination, carrier overflow, and hole transportation, surface recombination plays the most important role in the efficiency performance when the size of GaN/InGaN μ-LEDs shrinks down to a few microns. By setting up the parameters and structures of GaN/InGaN μ-LEDs in simulation tool APSYS, the simulation results corroborate this assertion and show that the IQE value decreases from 54% for 100×100 μm^2 devices to 5% for 5×5 μm^2 devices. The simulation results also exhibit that the IQE peak position shifts from 10 $A \cdot cm^{-2}$ for 100×100 μm^2 devices to >100 $A \cdot cm^{-2}$ for the 5×5 μm^2 devices. These simulation results provide a great reference to the new design of 5×5 μm^2 GaN/InGaN μ-LEDs for efficiency improvement.

Chapter 3 Simulation Reliability Confirmation: Temperature-dependent Efficiency Performance of GaN-Based μ-LEDs

3.1 Temperature-dependent Measurement

To verify the reliability of the simulation, our simulation results were compared to and confirmed by the experimental data measured from a 50×50 μm^2 μ-LED. The structure of the device is as shown in Figure 2.9. The detailed parameters of the device are the same as the information provided in section 2.4.1. The temperature-dependent efficiency performance and J-V characteristic are measured and compared with the simulation results.

3.1.1 Simulated and Measured J-V Characteristic

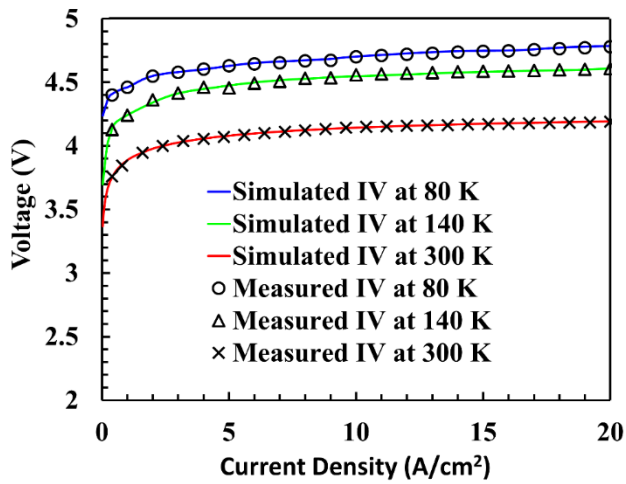

Figure 3.1 The measured curve compared to the simulated curve at different temperatures.

The temperature-dependent current-voltage characteristic curves of the device are plotted in Figure 3.1, which shows an excellent agreement between the simulation data in solid lines and experimental data in different symbols from 80 K to 300 K.

3.1.2 Simulated and Measured J-IQE (EQE) Characteristic

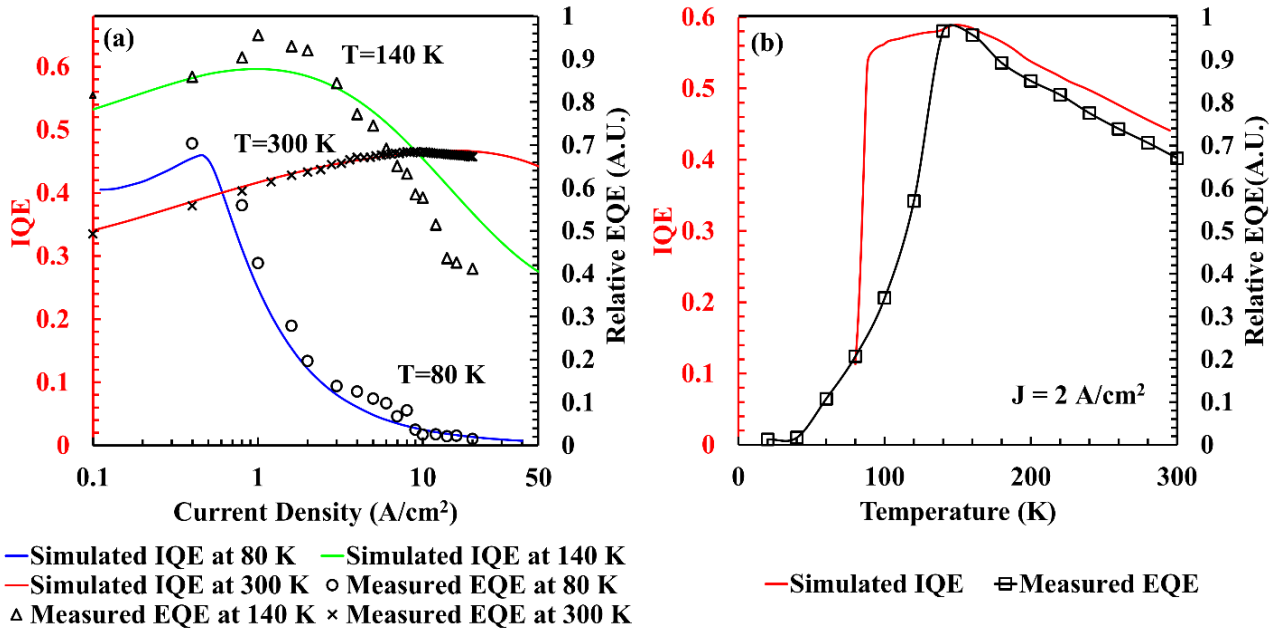

Figure 3.2 The measured EQE compared to the simulated IQE (a) current-density-dependent (in log-scale) efficiency at different temperatures (the measured current density range is from 0.4 to 20 A/cm^2); (b) temperature-dependent efficiency at 2A/cm^2.

Figure 3.2(a) shows the simulated and measured IQE (EQE) plots as a function of current density at different operating temperatures. We find a good agreement between the experimental data and the simulation result at 300 K and a reasonable agreement at low temperature from 80 K to 140 K with some deviation. The small discrepancies can be attributed to two reasons. Firstly, the simulated model in APSYS does not include the indium segregation phenomenon in the active region of a GaN/InGaN μ-LED. [63] Secondly, the p- or n-contacts in APSYS are considered as ohmic contacts and ignored the contact resistances. Figure 3.2(b) shows the measured relative EQE at different temperatures from 20 K up to 300 K at 2 A/cm^2 bias current density. As expected, when the temperature decreases from 300 K to 140 K, the relative EQE increases which is attributed to the reduction of non-radiative recombination fraction in the active region. However, when the temperature drops below 120 K, the EQE starts decreasing significantly.

3.2 Mechanisms for Degraded Performance of GaN/InGaN μ-LEDs at low temperature

The EQE deterioration at low temperature only occurs in GaN/InGaN μ-LEDs. For other optical devices, the efficiency performance at low temperature is well enhanced due to the reduction of non-radiative recombination fraction in the active region. Two mechanisms could account for this phenomenon: the fluctuation of Indium composition in the QWs and the high activation energy of Mg-acceptor Mg-doped p-type GaN.

3.2.1 The Fluctuation of Indium Composition in QWs

The fluctuation of indium composition was indicated by the blue- and red-shift in the EL spectrum of InGaN/GaN LEDs when the temperature decreases from 300 K to 5 K (shown in Figure 3.3). [64-67] Because indium tends to segregate into 2 - 3 nm clusters randomly, the optical emission efficiency of the LEDs suffers from this indium non-uniform distribution in the InGaN QW due to the carrier injection overflow. Thus, the efficiency degradation becomes more severe at low temperatures. [63,68] However, many other researchers believed that the indium cluster problem could be a good thing for the efficiency performance of GaN/InGaN μ-LEDs, as it allows defect-insensitive luminescence in InGaN QWs and LEDs regardless of the very high dislocation densities. Therefore, the properties of Indium may not be the major mechanism that account for the efficiency of GaN/InGaN μ-LEDs at low temperature.

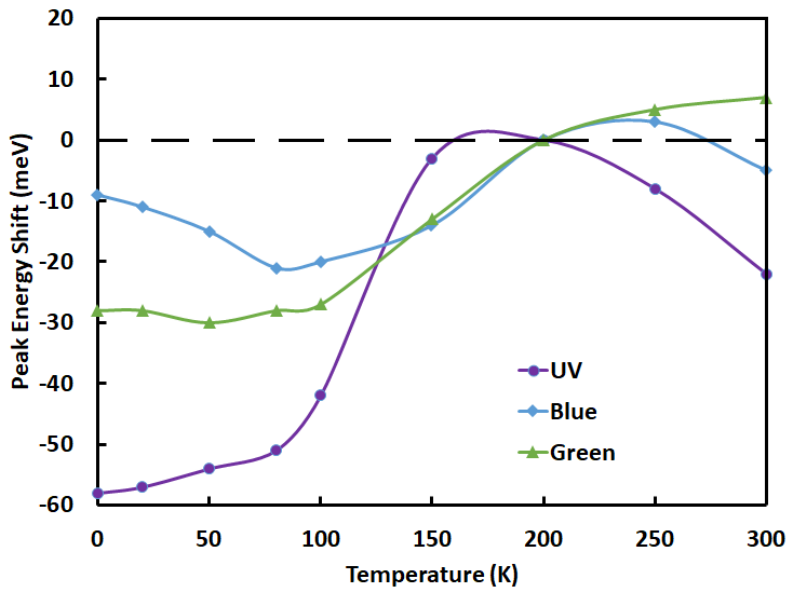

Figure 3.3 Values of peak energy shift as a function of temperature in different colors GaN/InGaN LEDs from [64].

3.2.2 High Activation Energy of Mg Acceptors Mg-doped p-type GaN and AlGaN

The major reason for the performance of GaN/InGaN μ-LEDs at low temperature is the the high activation energy of Mg acceptors in GaN (~0.15 eV) and AlGaN (~0.25 eV), [69-72]] which significantly decreases the activated acceptor concentration at lower temperature and results in rare activated acceptors and poor hole transportation in p-type region. As a result, the total device resistance increases which eventually leads to higher bias voltage requirement at same applied current density shown in Figure 3.1. On the other hand, the activation energy of Si donors (~0.02 eV) in GaN is comparatively low, [83] which results in abundance of activated donors and leads to good electron transportation at low temperature. This big number difference between holes and electrons shifts the recombination balance zone from QW's region to the p-type region and degrades IQE. This carrier imbalance is responsible for efficiency droop as well at high bias current density and low device temperature as shown in Figure 3.2.

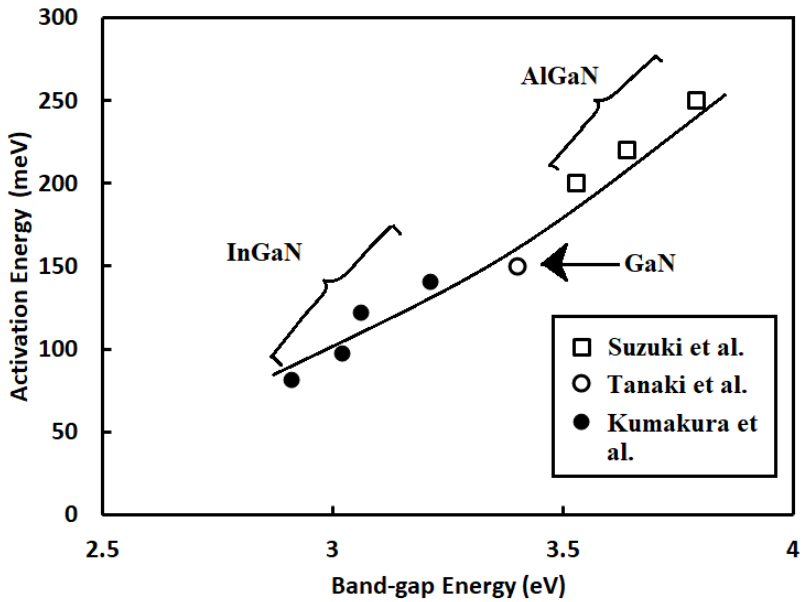

Figure 3.4 Activation energies of Mg acceptors in Mg-doped AlGaN, GaN, and InGaN as a function of the band-gap energies from reference [70-72].

3.3 Conclusion

The measured and simulated temperature-dependent efficiency performance of GaN/InGaN μ-LED exhibited good agreement with each other and proved the reliability of our simulation methods in this thesis. The major mechanism that explained the large degradation of the EQE below 150 K is the high activation energy (>0.15 eV) of the Mg acceptor in Mg-doped GaN and AlGaN, which is much higher than the activation energy (<0.02 eV) of the Si donor in Si-doped GaN. The big difference in carrier transportation of electrons and holes in GaN at low temperature results in the substantial efficiency drop.

Chapter 4 GaN-Based μ-LEDs with N-doped Quantum Barriers

4.1 μ-LEDs with Doped Quantum Barriers

4.1.1 The Structure of GaN/InGaN μ-LEDs with Doped Quantum Barriers

The common LED structure in Figure 2.9 has MQWs and quantum barriers. Normally, the GaN quantum barriers are undoped. However, sometimes researchers use doped GaN as the quantum barrier layers. It has been discovered that the GaN/InGaN μ-LEDs with doped quantum barriers can improve the efficiency performance at some working current density compared to the μ-LEDs with un-doped quantum barriers. Figure 4.1 shows the GaN/InGaN μ-LEDs with doped quantum barriers.

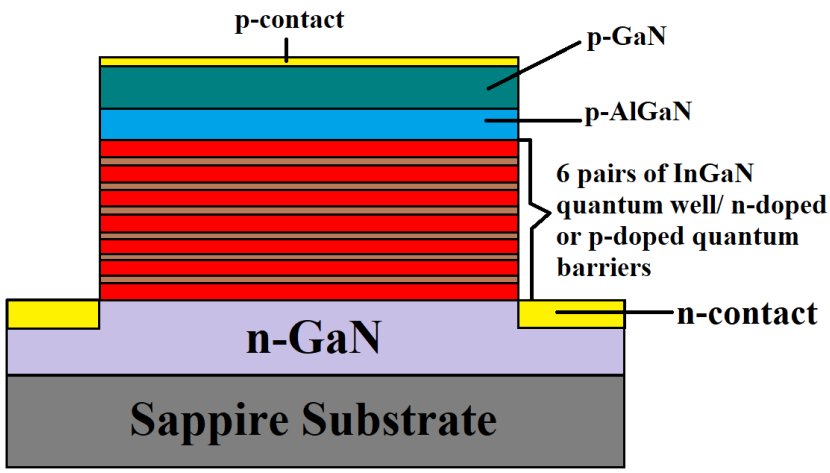

Figure 4.1 Structure of MQW GaN/InGaN μ-LEDs with doped quantum barriers.

4.1.2 GaN/InGaN μ-LEDs with P-doped Quantum Barriers

As mentioned in section 2.2.3, the hole transportation problem in GaN/InGaN limits the efficiency performance of GaN/InGaN μ-LEDs at higher injected current density. One of the popular methods for eliminating this problem is using p-doped quantum barriers. Han et al., [73] Xie et al. [74] and Ji et al. [75] respectively proved that p-doped quantum barriers can affect the hole transport

and distribution. Figure 4.2 exhibits the distribution of the holes in the QW active regions of GaN/InGaN μ-LEDs with and without p-doped quantum barriers. The hole distribution in the GaN/InGaN μ-LEDs with p-doped quantum barriers is more uniform, hence, the recombination center moves to the n-type layer.

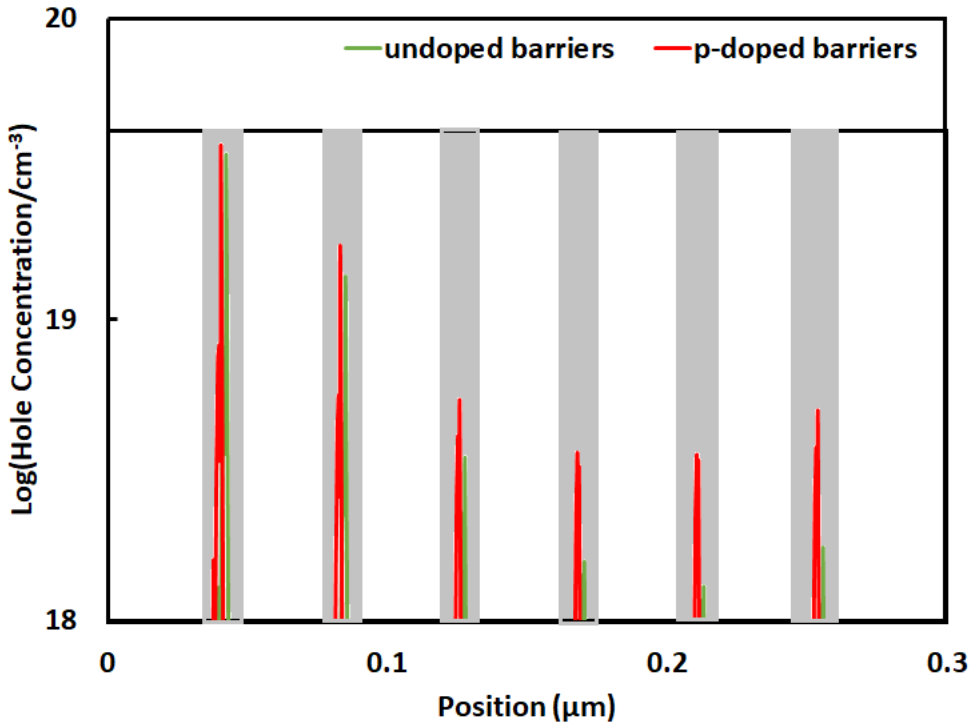

Figure 4.2 The hole distribution in the QW active regions of GaN/InGaN μ-LEDs with and without p-doped quantum barriers. The grey regions are the QWs.

4.1.3 GaN/InGaN μ-LEDs with N-doped Quantum Barriers

Due to the hole transportation drawback, most previous researches did not indicate any cases of GaN/InGaN LEDs with n-doped quantum barriers. Shi et al. [76,77] exhibited a kind of high-speed GaN/InGaN LEDs with n-doped quantum barriers. Otsuji et al. [78] and Takahashi et al. [79] also showed that GaN/InGaN LEDs with n-doped InGaN electron reservoir layers (ERL) have better performance at low temperature. Though none of these discoveries were related to efficiency performance.

In this work, we presented that GaN/InGaN μ-LED with n-doped quantum barriers can improve the efficiency of GaN/InGaN μ-LEDs in microns dimension (<10um). Although the hole transportation problem still exists at the micron levels GaN/InGaN μ-LEDs, this could be explained by analyzing the mechanism of the SRH recombination. The rate of the SRH

recombination is given in Eq. 2.3 we can slightly modify the expression of Eq. 2.3 into:

$$R_{SRH} = \frac{np - n_i^2}{\tau_p \frac{n}{f_n} + \tau_n \frac{p}{1-f_p}}, \quad (4.1)$$

Where f_n and f_p is the trap occupation probabilities (p for holes and n for electrons). With the same doping concentration, the SRH recombination rate in GaN/InGaN LEDs with n-doped or p-doped barriers are simplified to:

$$R_{SRH}^{n} = \frac{p_0 f_n}{\tau_p}, \quad (4.2)$$

$$R_{SRH}^{p} = \frac{n_0 (1-f_p)}{\tau_n}, \quad (4.3)$$

Where n_0 and p_0 are the electron and hole concentrations in the intrinsic GaN barrier layers and are approximately equal to each other. Since the trap occupation probabilities f_n in Eq. 4.2 and $1 - f_p$ in Eq. 4.3 roughly equals to each other as well, the SRH recombination rate is therefore inversely proportional to the SRH lifetime (τ_p or τ_n). In GaN, τ_p (about 7ns) [80] is much larger than τ_n (about 0.1ns). [81] Therefore, the SRH recombination rate R_{SRH}^{n} in devices with n-doped barriers is much smaller than those with p-doped barriers. For μ-LEDs with small dimension, the surface recombination, which is a kind of SRH recombination, becomes dominant in the efficiency performance because of the high surface areas to volumes ratio. Therefore, smaller R_{SRH}^{n} is the reason why GaN/InGaN μ-LEDs with n-doped barriers performs better than devices with undoped or p-doped barriers in small dimensions (less than 10um).

4.2 Simulation Results of GaN/InGaN μ-LEDs with Different Sizes and Different Doping Profile in Quantum Barriers

4.2.1 Efficiency Performance

Figure 4.3 shows the simulated IQE results of μ-LEDs with different dimensions (100×100, 50×50, 10×10, 5×5 μm^2) and quantum barriers with different doping profiles (intrinsic, p-doped at 5×10^{17} cm^{-3}, n-doped at 5×10^{17} cm^{-3}) at room temperature. The simulation results clearly showed that the IQE value significantly decreases as the device size shrinks, e. g., the peak IQE values drop from 49%-57% for 100×100 μm^2 (Fig. 4.3 (a)) to 2%-8% for 5×5 μm^2 (Fig. 4.3 (d)). Moreover, the IQE is strongly affected by doping profiles. As expected, larger-size devices with p-doped barrier layers (Fig. 4.3 (a) (b)) exhibit better performance in most of the common operation current density range (1 A/cm2 to 50 A/cm2) in comparison to counterparts with n-doped or intrinsic barriers. When the sizes shrink down to 10×10 μm^2 or below (Fig. 4.3 (c) and (d)), devices with n-doped barriers perform much better. The IQE value increase from 3.2%-4.5% for 5×5 μm^2 with undoped quantum barriers (Figure 4.3 (d) blue line) to 7.9%-6.5% for 5×5 μm^2 with undoped

quantum barriers (Figure 4.3 (d) red line).

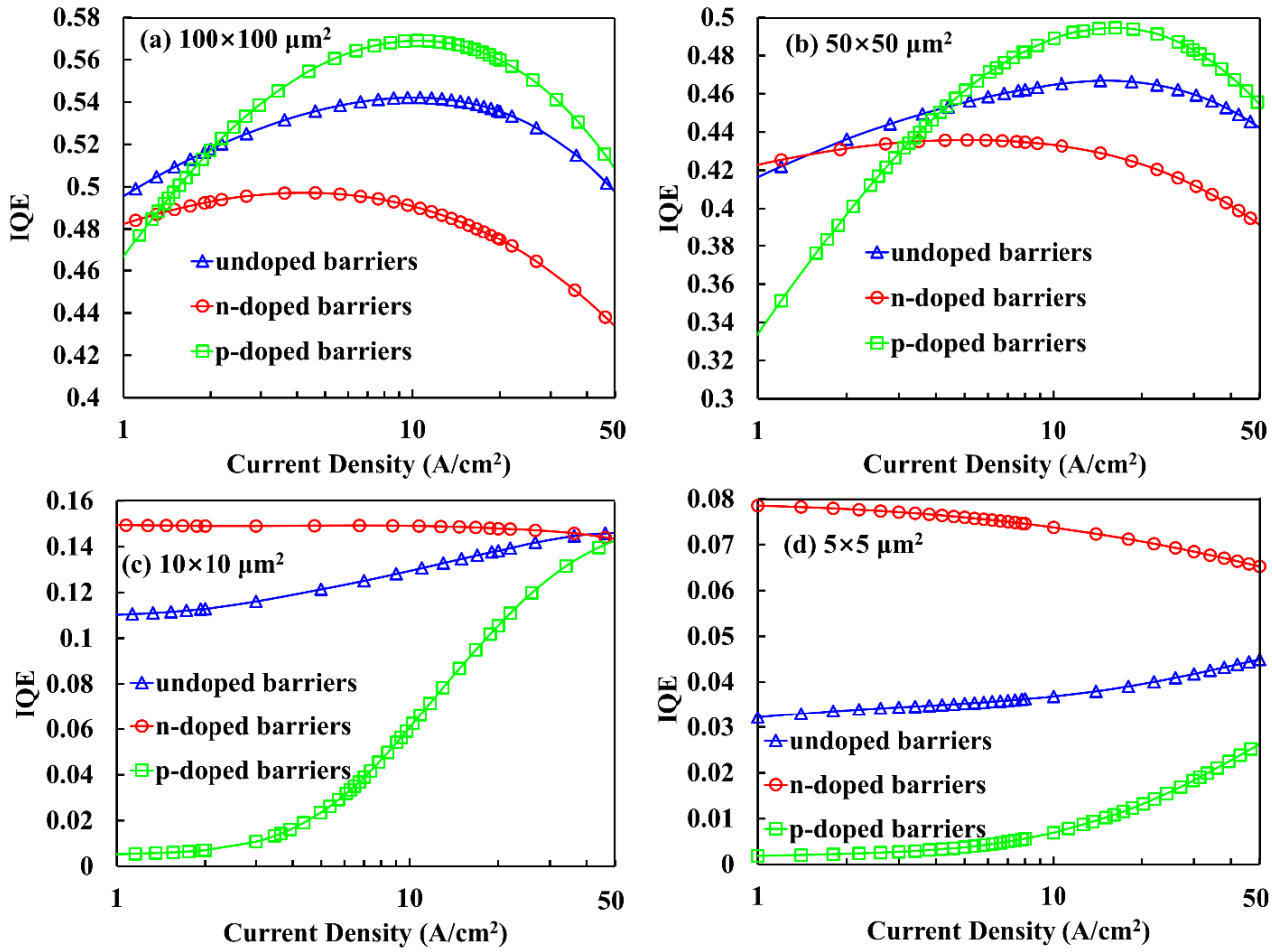

Figure 4.3 IQE as a function of current density (in log scale) curves of 4 different size μ-LEDs at room temperature with different doping profile (n-type or p-type doping concentration 5×10^{17} cm^{-3}) of barriers, (a) 100×100 μm^2 μ-LED, (b) 50×50 μm^2 μ-LED, (c) 10×10 μm^2 μ-LED, and (d) 5×5 μm^2 μ-LED.

4.2.2 Spatial SRH Recombination and Radiative Recombination Profiles

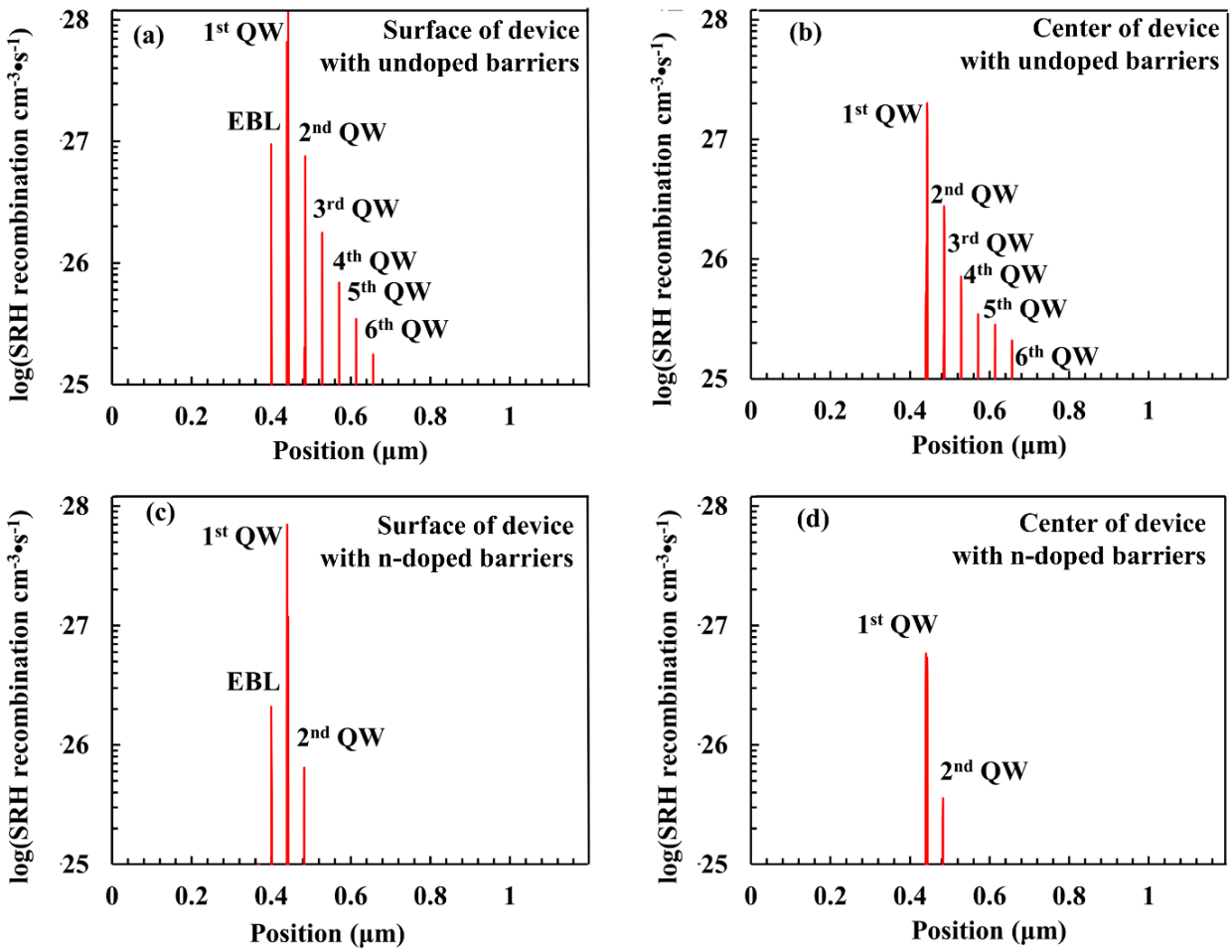

Figure 4.4 The simulated spatial distribution of SRH recombination profiles of a 5×5 μm^2 μ-LED at room temperature for 20A/cm^2 current density with undoped barriers at (a) surface, (b) center, with n-doped barriers at (c) surface, (d) center of the device.

The simulated spatial distribution of SRH recombination profiles are shown in Figure 4.4 for both n-doped (lower two plots) and undoped barriers (upper two plots). We find that the SRH recombination rate is substantially decreased both in surface and in center of the device with n-doped barriers. For example, SRH recombination rate drop approximately 40% in first QW from 1.18×10^{28} cm^{-3} s^{-1} (Figure 4.4(a)) to 6.91×10^{27} cm^{-3} s^{-1} (Figure 4.4(c)).

To understand the influence of number of QWs on device performance, we simulate the spatial radiative recombination rate by considering n-doped and undoped barriers. Figure 4.5 shows the

simulated spatial distribution of radiative recombination profiles of a 5×5 μm^2 GaN/InGaN μ-LED with undoped or n-doped barriers. We find that most of the radiative recombination occurs in the first QW near EBL in the center of the device, similar to that for SRH recombination case shown in Figure 4.4. The n-doped barriers can slightly increase the radiative recombination rate in the first QW in the center from 1.56×10^{27} cm^3 s^{-1} (Figure 4.5(b)) to 2.36×10^{27} cm^3 s^{-1} (Figure 4.5(d)), and decrease in other QWs.

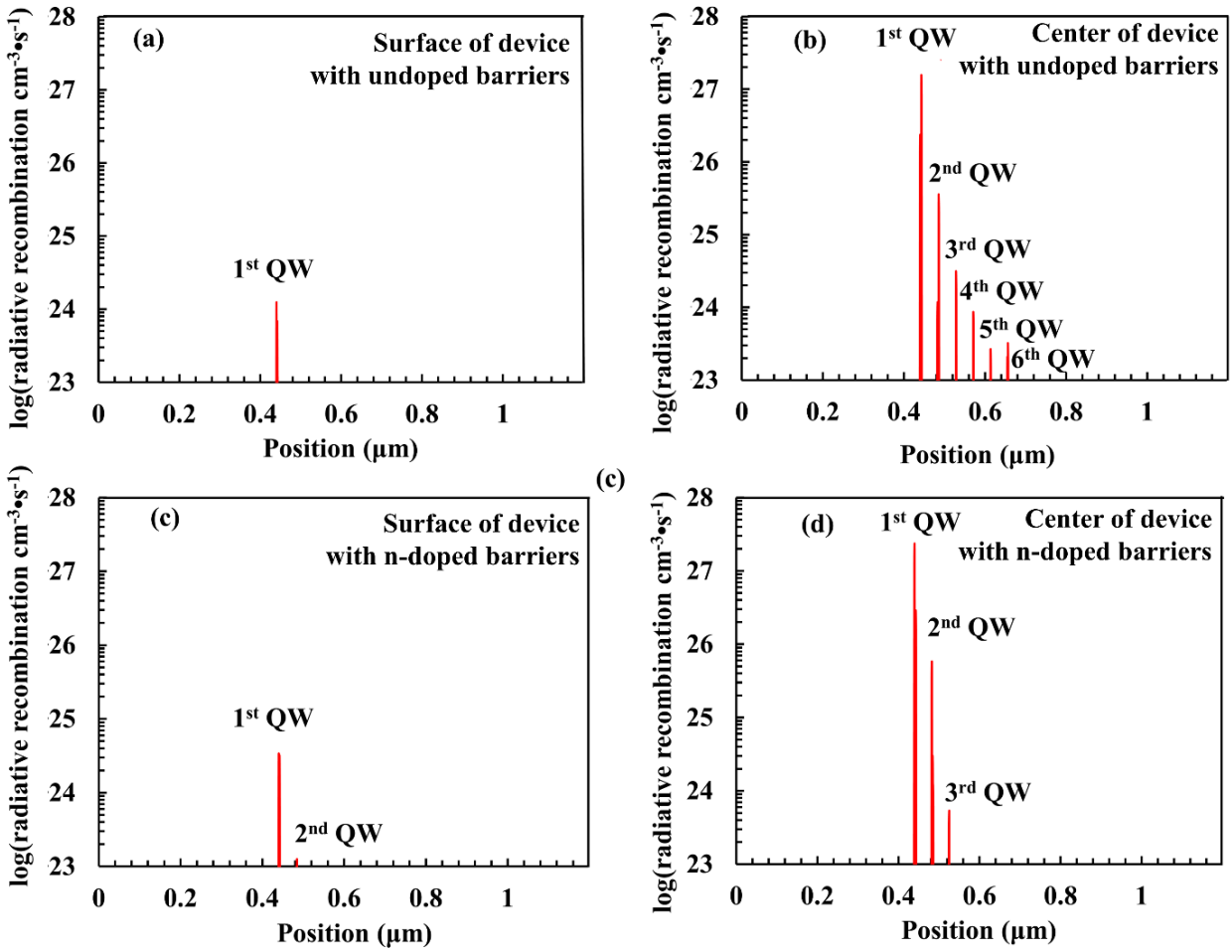

Figure 4.5 The simulated spatial distribution of radiative recombination profiles of a 5×5 μm2 μ-LED at room temperature for 20A/cm^2 current density with undoped barriers at (a) surface, (b) center, with n-doped barriers at (c) surface, (d) center of the device.

To easily understand, here we use the IQE model (Eq. 2.8) and safely neglect the Auger term. The IQE in QWs is given by:

$$\eta_{IQE,QWs} \approx \frac{R_{rad}}{R_{SRH}+R_{rad}}. \tag{4.4}$$

In Table 4.1, we show the IQE in the surface and center of different QW regions in a 5×5 μm^2 GaN/InGaN μ-LED with undoped and n-doped quantum barriers. We can see that the IQE in the

center of the first QW with undoped barriers or n-doped barriers is much higher than the IQE in the center of the other QWs. In the surface of the QWs with undoped barriers or n-doped barriers, the IQE is almost 0%. Therefore, 5×5 μm^2 GaN/InGaN μ-LEDs with only one QW should have the better performance compared to the MQWs structure.

Position	IQE in the surface of QWs with undoped barriers	IQE in the center of QWs with undoped barriers	IQE in the surface of QWs with n-doped barriers	IQE in the center of QWs with n-doped barriers
1st QW	0.0%	43.8%	0.0%	80.2%
2nd QW	0.0%	11.5%	0.2%	62.0%
3rd QW	0.0%	4.2%	0.3%	61.2%
4th QW	0.0%	2.4%	0.3%	61.3%
5th QW	0.0%	0.9%	0.3%	61.3%
6th QW	0.0%	1.5%	0.5%	61.3%

Table 4.1 The IQE in the surface and center of different QW regions in a 5×5 μm^2 GaN/InGaN μ-LED with undoped and n-doped quantum barriers

4.2.3 Efficiency Optimization for 5×5 μm^2 GaN/InGaN μ-LEDs

Although, n-doped barriers are capable of improving the efficiency of GaN/InGaN μ-LEDs, it will aggravate the unbalanced electron-hole injection problem and push the recombination zone close to the p-GaN region. As a consequence, high doping concentration in the n-doped barriers will cause the efficiency droop problem. However, this problem can be carefully avoided by tuning the doping concentration in the n-doped barriers which is a tradeoff between balancing the electron/holes injection and suppressing the non-radiative SRH recombination. Figure 5 shows the simulated IQE of a 5×5 μm^2 μ-LED with varying n-type doping concentration in the barriers. The optimum doping concentration is estimated to be 5×10^{17} cm^{-3} in the barriers which exhibits the overall highest IQE in the range of bias current density.

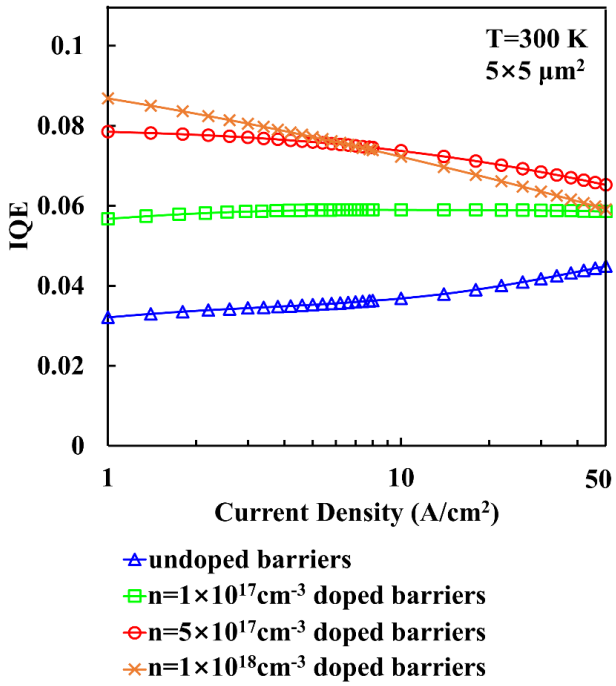

Figure 4.6 The IQE as a function of current density. (in log scale) curves of GaN/InGaN μ-LEDs with different n-doping concentrations in quantum barriers at room temperature.

To finally optimize the efficiency performance of the 5×5 μm^2 μ-LED, a series of 5×5 μm^2 μ-LEDs with a single, 3 and 6 QWs and n-doped barriers were simulated. Compared to devices with MQWs, the single QW LED (shown in Figure 4.8) has the lowest surface area to volume ratio and exhibits the best performance due to the minimized surface recombination. The simulation results as shown in Fig. 4.7 revealed that the optimized design can improve the IQE by more than 100% in comparison to a convention design with intrinsic MQWs active regions in working current density range. At 1 A/cm^2, the IQE reaches 11% which is close to the commercial requirement of the GaN/InGaN μ-LEDs (15%).

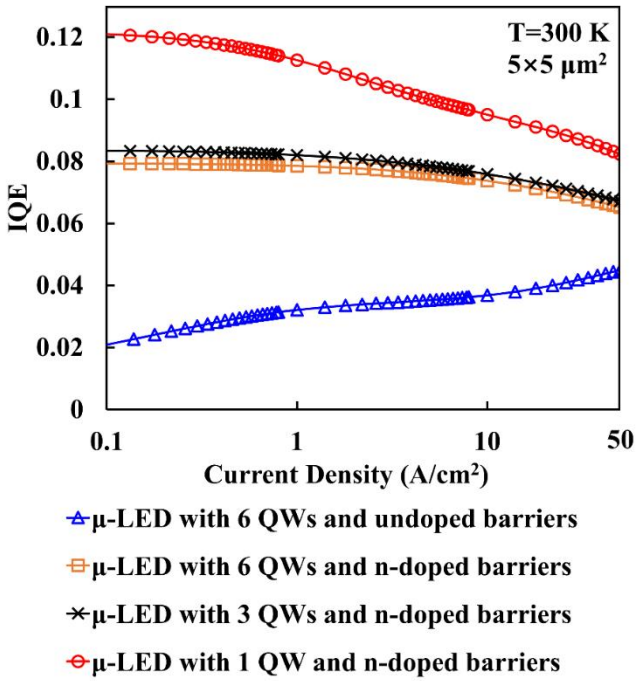

Figure 4.7 The current-density-dependent (in log sc•le) efficiency performance between the optimized μ-LED (1, 3, 6 QWs with 5×10^{17} cm^{-3} n-doped barriers) and conventional μ-LED (6 QWs with intrinsic barriers) of the 5×5 μm^2 GaN/InGaN μ-LEDs.

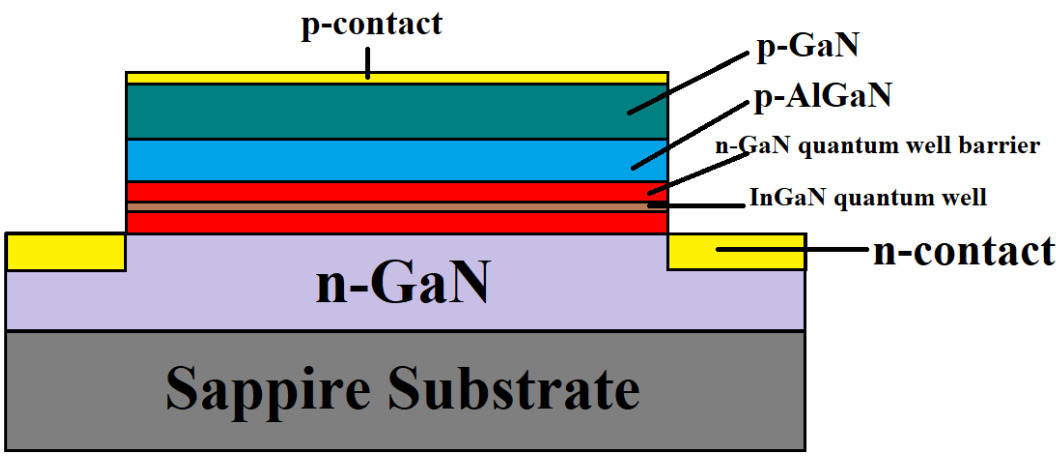

Figure 4.8 Structure of a single QW GaN/InGaN μ-LEDs with n-doped quantum barriers.

4.2.4 Simulated J-V Characteristic of 5×5 μm² GaN/InGaN μ-LEDs with Different Doping Profiles in Quantum Barriers

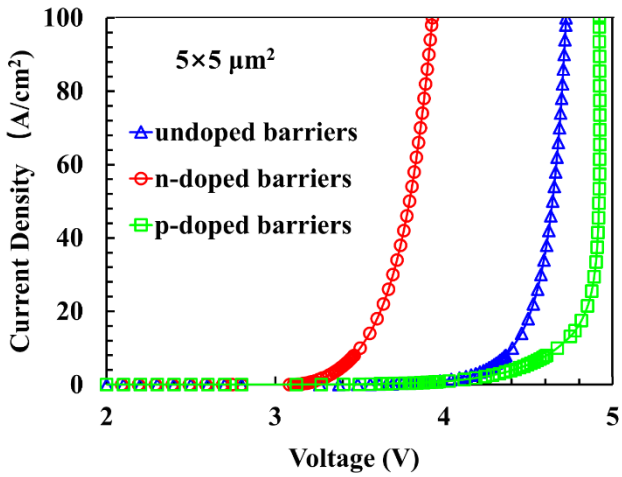

Figure 4.9 The j-V curve of the 5×5 μm² GaN/InGaN μ-LED with different doping profile (intrinsic, p-doped at 5×10^{17} cm^{-3}, n-doped at 5×10^{17} cm^{-3}) in quantum barriers.

Figure 4.9 shows the j-V curve of the 5×5 μm² GaN/InGaN μ-LED with different doping profile (intrinsic, p-doped at 5×10^{17} cm^{-3}, n-doped at 5×10^{17} cm^{-3}) in quantum barriers. From the figure, we can observe that the turn-on voltage of GaN/InGaN μ-LED with n-doped quantum barriers is smaller than the turn-on voltage of GaN/InGaN μ-LED with undoped or p-doped barriers. To easily understand, the IV characteristic of a general p-n junction is given by:

$$\mathrm{I} = I_s(e^{qV/kT} - 1), \tag{4.5}$$

where q is the charge of an electron, k is the Boltzmann constant and T is the temperature of the device. I_s is called the reverse saturation current of the diode and given by:

$$I_s = Aqn_i^2\left(\frac{D_p}{N_D w_n} + \frac{D_n}{N_A w_p}\right), \tag{4.6}$$

where A is the cross-section of the device, n_i is the intrinsic carrier concentration, $D_{p,n}$ are the diffusion coefficient of electrons and holes, $N_{D,A}$ are the concentration of acceptors and donors, and $w_{n,p}$ are the effective width of the n-layer and p-layer. In a p+/n junction ($N_A >> N_D$):

$$I_s = Aqn_i^2\left(\frac{D_p}{N_D w_n}\right). \tag{4.7}$$

In an n+/p junction ($N_D >> N_A$):

$$I_s = Aqn_i^2\left(\frac{D_n}{N_A w_p}\right). \tag{4.8}$$

According to Einstein relation, the diffusion coefficient is proportional to the mobility. Because the hole mobility is much smaller than electron mobility in GaN, D_p is much smaller than D_n. Therefore, I_s in device with p-doped barriers is smaller than I_s in device with n-doped barriers. To

reach the same current with smaller I_s, higher voltage bias is required. That is why the turn-on voltage of GaN/InGaN μ-LED with n-doped quantum barriers is smaller than the turn-on voltage of GaN/InGaN μ-LED with undoped or p-doped barriers.

4.3 Conclusion

In summary, the size-dependent efficiency performance of GaN/InGaN μ-LEDs with different doping file in quantum barriers has been investigated by simulation. The analysis shows that GaN/InGaN μ-LEDs with p-doped quantum barriers have better performance when the size is larger than 50μm due to the compensation for hole transportation. It was also shown that when the size shrinks down below 10μm, GaN/InGaN μ-LEDs with n-doped quantum barriers exhibited better efficiency performance compared to the undoped quantum barriers and p-doped quantum barriers. The IQE improvement of devices with n-doped quantum barriers is more than 100% compared to the IQE of devices with undoped quantum barriers. The doping concentration and in n-doped quantum barriers and the number of quantum wells of GaN/InGaN μ-LEDs can be optimized with a tradeoff between balancing electron/holes transportation and suppressing the non-radiative SRH recombination. Our simulation results showed that a device designed with n-doped barriers and single QW structure can significantly improve the IQE of a 5×5 μm^2 GaN/InGaN μ-LEDs by more than 100% compared to the conventional MQW LEDs with intrinsic active regions. The 11% IQE value of 5×5 μm^2 GaN/InGaN μ-LEDs at $1A\bullet cm^{-2}$ is very close to 15%, which is the satisfied IQE value for commercial use.

Chapter 5 Conclusion and Future Work

This thesis reports a comprehensive study on GaN/InGaN μ-LEDs. The APSYS simulation software is used to simulate the efficiency performance and other electric characterization of GaN/InGaN μ-LEDs. The mechanisms that affect the efficiency performance of the GaN/InGaN μ-LEDs are explained. In small size (<10m) GaN/InGaN μ-LEDs, the surface recombination rate begins to play a critical role in the efficiency of the GaN/InGaN μ-LEDs due to the high surface area to volume ratio of the device.

Simulation results are compared with the experimental data measured from a 50×50 μm^2 μ-LED. The measured results and simulated results show close trends with each other. The phenomenon when the EQE (IQE) dramatically decreases at low temperature can be attributed to the high activation energy of Mg acceptor in the Mg-doped active region.

To suppress the surface recombination effect and improve the efficiency performance of the GaN/InGaN μ-LEDs, a novel LED structure with n-doped quantum barriers is demonstrated. According to earlier research work, the p-doped quantum barriers have been proven to enhance the hole transportation in GaN/InGaN μ-LEDs and alleviate the efficiency droop problem. However, based on the new model presented in this thesis, the SRH recombination (surface recombination) in n-doped layer is much smaller than that in p-doped layer. Therefore, GaN/InGaN μ-LEDs with n-doped quantum barriers can effectively suppress the surface recombination and improve the quantum efficiency. By optimizing the doping concentration of the n-doped barriers with a tradeoff between balancing electron and holes injection and suppressing the non-radiative SRH recombination, a designed 5×5 μm^2 GaN/InGaN μ-LED structure with a single QW and n-doped barriers is presented. The simulation results show that the new design exhibits a more than 100% efficiency improvement at 20$A \cdot cm^{-2}$ compared to the conventional intrinsic MQWs based design.

In conclusion, a comprehensive study of GaN/InGaN μ-LEDs is reported in this thesis, in which, new devise work mechanism, simulation and experimental results are presented. A newly designed GaN/InGaN μ-LED with n-doped quantum barriers is demonstrated.

There are some clear future works:

1. Further examination on working mechanism of GaN/InGaN μ-LED with n-doped quantum barriers should be conducted. Based on the n-doped quantum barriers, device will be grown, fabricated, and tested.

2. The efficiency drop of the GaN/InGaN μ-LED at low temperature needs to be further

investigated. The positive charge induced by temperature dependent polarization effect, is expected to replace the Mg acceptors in p-type GaN/InGaN.

3. For GaN/InGaN LEDs with larger sizes, some inherent drawbacks are required to be addressed. For example, the carrier overflow drawbacks can be surmounted by using a bottom tunnel junction structure to reverse the p- and n-GaN layer. For GaN/InGaN LEDS with very small size, the EQE value could be improved to almost 15% and made available at cost-effective value.

4. The value of SRV typically ranges from 10^5 to 10^7 cm/s in red LEDs, like GaAsP based LED. It is much higher than the value in GaN/InGaN LEDs, which causes a more significant efficiency drop in red μ-LEDs. In future, we plan to investigate the effect of doping profile in QW barriers of μ-LEDs with different materials.

References

[1] Okon, T. M., & Biard, J. R. (2015). The first practical LED. *Edison Tech Center*, 1-14.

[2] Holonyak Jr, N., & Bevacqua, S. F. (1962). Coherent (visible) light emission from Ga (As1− x P x) junctions. *Applied Physics Letters*, *1*(4), 82-83.

[3] Losev, O., Biard, J. R., & Holonyak, N. (2016). Light-emitting diode.

[4] Patel, N. V. (2014). Nobel shocker: RCA had the first blue LED in 1972. *IEEE Spectrum*.

[5] Shen, Y. C., Mueller, G. O., Watanabe, S., Gardner, N. F., Munkholm, A., & Krames, M. R. (2007). Auger recombination in InGaN measured by photoluminescence. *Applied Physics Letters*, *91*(14), 141101.

[6] Kioupakis, E., Rinke, P., Delaney, K. T., & Van de Walle, C. G. (2011). Indirect Auger recombination as a cause of efficiency droop in nitride light-emitting diodes. *Applied Physics Letters*, *98*(16), 161107.

[7] Wang, C. H., Ke, C. C., Lee, C. Y., Chang, S. P., Chang, W. T., Li, J. C., ... & Wang, S. C. (2010). Hole injection and efficiency droop improvement in InGaN/GaN light-emitting diodes by band-engineered electron blocking layer. *Applied Physics Letters*, *97*(26), 261103.

[8] Choi, S., Ji, M. H., Kim, J., Jin Kim, H., Satter, M. M., Yoder, P. D., ... & Ponce, F. A. (2012). Efficiency droop due to electron spill-over and limited hole injection in III-nitride visible light-emitting diodes employing lattice-matched InAlN electron blocking layers. *Applied Physics Letters*, *101*(16), 161110.

[9] Vampola, K. J., Iza, M., Keller, S., DenBaars, S. P., & Nakamura, S. (2009). Measurement of electron overflow in 450 nm InGaN light-emitting diode structures. *Applied Physics Letters*, *94*(6), 061116.

[10] Wen, B., Xu, C., Wang, S., Wang, K., Tam, M. C., Wasilewski, Z., & Ban, D. (2018). Dual-lasing channel quantum cascade laser based on scattering-assisted injection design. *Optics express*, *26*(7), 9194-9204.

[11] Jin, S. X., Li, J., Lin, J. Y., & Jiang, H. X. (2000). InGaN/GaN quantum well interconnected microdisk light emitting diodes. *Applied Physics Letters*, *77*(20), 3236-3238

[12] Pong, B. J., Chen, C. H., Hsu, J. F., Tun, C. J., & Chi, G. C. (2005, September). Electro-ridge for large injection current of micro-size InGaN light emitting diode. In *Fifth International Conference on Solid State Lighting* (Vol. 5941, p. 59410Y). International Society for Optics and Photonics.

[13] Tian, P., McKendry, J. J., Gong, Z., Guilhabert, B., Watson, I. M., Gu, E., ... & Dawson, M. D. (2012). Size-dependent efficiency and efficiency droop of blue InGaN micro-light emitting diodes. *Applied Physics Letters*, *101*(23), 231110.

[14] Nakamura, S., & Chichibu, S. F. (2000). *Introduction to nitride semiconductor blue lasers and light emitting diodes*. CRC Press.

[15] Nakamura, S., Mukai, T., & Senoh, M. (1994). Candela-class high-brightness InGaN/AlGaN

double-heterostructure blue-light-emitting diodes. *Applied Physics Letters*, *64*(13), 1687-1689.
[16] Nakamura, S., Mukai, T., & Senoh, M. (1994). High-brightness InGaN/AlGaN double-heterostructure blue-green-light-emitting diodes. *Journal of Applied Physics*, *76*(12), 8189-8191.
[17] Bernanose, A., Comte, M., & Vouaux, P. (1953). A new method of emission of light by certain organic compounds. *J. Chim. Phys*, *50*, 64-68.
[18] Bernanose, A., & Vouaux, P. (1953). Organic electroluminescence type of emission. *J. Chim. Phys*, *50*, 261.
[19] Bernanose, A. (1955). The mechanism of organic electroluminescence. *Journal of Chemical Physics*, *52*, 396-400.
[20] Bernanose, A., Comte, M., & Vouaux, P. (1955). Organic phosphorescence. *Bull. Soc. Pharm. Nancy*, *26*, 5-11.
[21] Helfrich, W., & Schneider, W. G. (1965). Recombination radiation in anthracene crystals. *Physical Review Letters*, *14*(7), 229.
[22] Vincett, P. S., Barlow, W. A., Hann, R. A., & Roberts, G. G. (1982). Electrical conduction and low voltage blue electroluminescence in vacuum-deposited organic films. *Thin solid films*, *94*(2), 171-183.
[23] Tang, C. W., & VanSlyke, S. A. (1987). Organic electroluminescent diodes. *Applied physics letters*, *51*(12), 913-915.
[24] Chin, B. D., Choi, Y., Baek, H. I., & Lee, C. (2009, August). High efficiency phosphorescent OLEDs based on the heterostructured light emission and charge injection layers. In *Organic Light Emitting Materials and Devices XIII* (Vol. 7415, p. 741510). International Society for Optics and Photonics
[25] Baldo, M. A., O'brien, D. F., You, Y., Shoustikov, A., Sibley, S., Thompson, M. E., & Forrest, S. R. (1998). Highly efficient phosphorescent emission from organic electroluminescent devices. *Nature*, *395*(6698), 151.
[26] Baldo, M., Lamansky, S., Burrows, P., Thompson, M., & Forrest, S. (1999). Very high-efficiency green organic light-emitting devices based on electrophosphorescence. *Applied Physics Letters*, *75*(1), 4-6.
[27] Endo, A., Ogasawara, M., Takahashi, A., Yokoyama, D., Kato, Y., & Adachi, C. (2009). Thermally activated delayed fluorescence from Sn4+–porphyrin complexes and their application to organic light emitting diodes—A novel mechanism for electroluminescence. *Advanced Materials*, *21*(47), 4802-4806.
[28] Goushi, K., Yoshida, K., Sato, K., & Adachi, C. (2012). Organic light-emitting diodes employing efficient reverse intersystem crossing for triplet-to-singlet state conversion. *Nature Photonics*, *6*(4), 253.
[29] Zhang, Q., Li, B., Huang, S., Nomura, H., Tanaka, H., & Adachi, C. (2014). Efficient blue organic light-emitting diodes employing thermally activated delayed fluorescence. *Nature Photonics*, *8*(4), 326.
[30] Pollentier, I., Demeester, P., Ackaert, A., Buydens, L., Van Daele, P., & Baets, R. (1990). Epitaxial lift-off GaAs LEDs to Si for fabrication of opto-electronic integrated circuits. *Electronics Letters*, *26*(3), 193-194.

[31] Wong, W. S., Sands, T., Cheung, N. W., Kneissl, M., Bour, D. P., Mei, P., ... & Johnson, N. M. (2000). In x Ga 1− x N light emitting diodes on Si substrates fabricated by Pd–In metal bonding and laser lift-off. *Applied Physics Letters*, *77*(18), 2822-2824.
[32] Pong, B. J., Chen, C. H., Hsu, J. F., Tun, C. J., & Chi, G. C. (2005, September). Electro-ridge for large injection current of micro-size InGaN light emitting diode. In *Fifth International Conference on Solid State Lighting* (Vol. 5941, p. 59410Y). International Society for Optics and Photonics.
[33] Jiang, H. X., Jin, S. X., Li, J., Shakya, J., & Lin, J. Y. (2001). III-nitride blue microdisplays. *Applied Physics Letters*, *78*(9), 1303-1305.
[34] Choi, H. W., Jeon, C. W., Dawson, M. D., Edwards, P. R., & Martin, R. W. (2003). Fabrication and performance of parallel-addressed InGaN micro-LED arrays. *IEEE Photonics Technology Letters*, *15*(4), 510-512.
[35] Choi, H. W., Jeon, C. W., Dawson, M. D., Edwards, P. R., Martin, R. W., & Tripathy, S. (2003). Mechanism of enhanced light output efficiency in InGaN-based microlight emitting diodes. *Journal of Applied Physics*, *93*(10), 5978-5982.
[36] Jin, S. X., Li, J., Lin, J. Y., & Jiang, H. X. (2000). InGaN/GaN quantum well interconnected microdisk light emitting diodes. *Applied Physics Letters*, *77*(20), 3236-3238.
[37] Dupré, L., Marra, M., Verney, V., Aventurier, B., Henry, F., Olivier, F., ... & Templier, F. (2017, February). Processing and characterization of high resolution GaN/InGaN LED arrays at 10 micron pitch for micro display applications. In *Gallium Nitride Materials and Devices XII* (Vol. 10104, p. 1010422). International Society for Optics and Photonics.
[38] Tian, P., McKendry, J. J., Gong, Z., Guilhabert, B., Watson, I. M., Gu, E., ... & Dawson, M. D. (2012). Size-dependent efficiency and efficiency droop of blue InGaN micro-light emitting diodes. *Applied Physics Letters*, *101*(23), 231110.
[39] Li, S. S. (2012). *Semiconductor physical electronics*. Springer Science & Business Media
[40] Shockley, W. T. R. W., & Read Jr, W. T. (1952). Statistics of the recombinations of holes and electrons. *Physical review*, *87*(5), 835.
[41] Piprek, J. (2010). Efficiency droop in nitride-based light-emitting diodes. *physica status solidi (a)*, *207*(10), 2217-2225.
[42] Poher, V., Grossman, N., Kennedy, G. T., Nikolic, K., Zhang, H. X., Gong, Z., ... & Degenaar, P. (2008). Micro-LED arrays: a tool for two-dimensional neuron stimulation. *Journal of Physics D: Applied Physics*, *41*(9), 094014.
[43] Grossman, N., Poher, V., Grubb, M. S., Kennedy, G. T., Nikolic, K., McGovern, B., ... & Dawson, M. D. (2010). Multi-site optical excitation using ChR2 and micro-LED array. *Journal of neural engineering*, *7*(1), 016004.
[44] López-Gejo, J., Navarro-Tobar, Á., Arranz, A., Palacio, C., Muñoz, E., & Orellana, G. (2011). Direct grafting of long-lived luminescent indicator dyes to GaN light-emitting diodes for chemical microsensor development. *ACS applied materials & interfaces*, *3*(10), 3846-3854.
[45] Jiang, H. X., Jin, S. X., Li, J., Shakya, J., & Lin, J. Y. (2001). III-nitride blue microdisplays. *Applied Physics Letters*, *78*(9), 1303-1305.
[46] Day, J., Li, J., Lie, D. Y. C., Bradford, C., Lin, J. Y., & Jiang, H. X. (2011). III-Nitride full-

scale high-resolution microdisplays. *Applied Physics Letters*, *99*(3), 031116.
[47] Iveland, J., Martinelli, L., Peretti, J., Speck, J. S., & Weisbuch, C. (2013). Direct measurement of Auger electrons emitted from a semiconductor light-emitting diode under electrical injection: identification of the dominant mechanism for efficiency droop. *Physical review letters*, *110*(17), 177406.
[48] Wood, C., & Jena, D. (Eds.). (2007). *Polarization effects in semiconductors: from ab initio theory to device applications*. Springer Science & Business Media.
[49] Kim, M. H., Schubert, M. F., Dai, Q., Kim, J. K., Schubert, E. F., Piprek, J., & Park, Y. (2007). Origin of efficiency droop in GaN-based light-emitting diodes. *Applied Physics Letters*, *91*(18), 183507.
[50] Turski, H., Bharadwaj, S., Xing, H., & Jena, D. (2019). Polarization control in nitride quantum well light emitters enabled by bottom tunnel-junctions. *Journal of Applied Physics*, *125*(20), 203104.
[51] Mnatsakanov, T. T., Levinshtein, M. E., Pomortseva, L. I., Yurkov, S. N., Simin, G. S., & Khan, M. A. (2003). Carrier mobility model for GaN. *Solid-State Electronics*, *47*(1), 111-115.
[52] Xie, J., Ni, X., Fan, Q., Shimada, R., Özgür, Ü., & Morkoç, H. (2008). On the efficiency droop in InGaN multiple quantum well blue light emitting diodes and its reduction with p-doped quantum well barriers. *Applied Physics Letters*, *93*(12), 121107.
[53] Choi, S., Ji, M. H., Kim, J., Jin Kim, H., Satter, M. M., Yoder, P. D., ... & Ponce, F. A. (2012). Efficiency droop due to electron spill-over and limited hole injection in III-nitride visible light-emitting diodes employing lattice-matched InAlN electron blocking layers. *Applied Physics Letters*, *101*(16), 161110.
[54] Mukai, T., Yamada, M., & Nakamura, S. (1999). Characteristics of InGaN-based UV/blue/green/amber/red light-emitting diodes. *Japanese Journal of Applied Physics*, *38*(7R), 3976.
[55] Bulashevich, K. A., & Karpov, S. Y. (2016). Impact of surface recombination on efficiency of III-nitride light-emitting diodes. *physica status solidi (RRL)–Rapid Research Letters*, *10*(6), 480-484.
[56] Jin, S. X., Li, J., Lin, J. Y., & Jiang, H. X. (2000). InGaN/GaN quantum well interconnected microdisk light emitting diodes. *Applied Physics Letters*, *77*(20), 3236-3238.
[57] Pong, B. J., Chen, C. H., Hsu, J. F., Tun, C. J., & Chi, G. C. (2005, September). Electro-ridge for large injection current of micro-size InGaN light emitting diode. In *Fifth International Conference on Solid State Lighting* (Vol. 5941, p. 59410Y). International Society for Optics and Photonics.
[58] Konoplev, S. S., Bulashevich, K. A., & Karpov, S. Y. (2018). From large-size to micro-LEDs: scaling trends revealed by modeling. *physica status solidi (a)*, *215*(10), 1700508.
[59] Bulashevich, K., Konoplev, S., & Karpov, S. (2018). Effect of Die Shape and Size on Performance of III-Nitride Micro-LEDs: A Modeling Study. In *Photonics* (Vol. 5, No. 4, p. 41). Multidisciplinary Digital Publishing Institute.
[60] Zhang, S., Li, Y., Fathololoumi, S., Nguyen, H. P. T., Wang, Q., Mi, Z., ... & Wang, G. T. (2013). On the efficiency droop of top-down etched InGaN/GaN nanorod light emitting diodes

under optical pumping. *AIP Advances*, *3*(8), 082103.
[61] Tian, P., McKendry, J. J., Gong, Z., Guilhabert, B., Watson, I. M., Gu, E., ... & Dawson, M. D. (2012). Size-dependent efficiency and efficiency droop of blue InGaN micro-light emitting diodes. *Applied Physics Letters*, *101*(23), 231110.
[62] APSYS, C. (2010). technical manuals. Crosslight Software, Inc., Burnaby, Canada.
[63] Gu, G. H., Park, C. G., & Nam, K. B. (2009). Inhomogeneity of a highly efficient InGaN based blue LED studied by three-dimensional atom probe tomography. *physica status solidi (RRL)–Rapid Research Letters*, *3*(4), 100-102.
[64] Cao, X. A., LeBoeuf, S. F., Rowland, L. B., Yan, C. H., & Liu, H. (2003). Temperature-dependent emission intensity and energy shift in InGaN/GaN multiple-quantum-well light-emitting diodes. *Applied Physics Letters*, *82*(21), 3614-3616.
[65] Cho, Y. H., Gainer, G. H., Fischer, A. J., Song, J. J., Keller, S., Mishra, U. K., & DenBaars, S. P. (1998). "S-shaped" temperature-dependent emission shift and carrier dynamics in InGaN/GaN multiple quantum wells. *Applied Physics Letters*, *73*(10), 1370-1372.
[66] Teo, K. L., Colton, J. S., Yu, P. Y., Weber, E. R., Li, M. F., Liu, W., ... & Matsumoto, K. (1998). An analysis of temperature dependent photoluminescence line shapes in InGaN. *Applied physics letters*, *73*(12), 1697-1699.
[67] Shin, D. S., Han, D. P., Oh, J. Y., & Shim, J. I. (2012). Study of droop phenomena in InGaN-based blue and green light-emitting diodes by temperature-dependent electroluminescence. *Applied Physics Letters*, *100*(15), 153506.
[68] Eliseev, P. G., Osin'ski, M., Li, H., & Akimova, I. V. (1999). Recombination balance in green-light-emitting GaN/InGaN/AlGaN quantum wells. *Applied Physics Letters*, *75*(24), 3838-3840.
[69] Lee, C. M., Chuo, C. C., Dai, J. F., Zheng, X. F., & Chyi, J. I. (2001). Temperature dependence of the radiative recombination zone in InGaN/GaN multiple quantum well light-emitting diodes. *Journal of Applied Physics*, *89*(11), 6554-6556.
[70] Kumakura, K., Makimoto, T., & Kobayashi, N. (2000). Activation energy and electrical activity of Mg in Mg-doped InxGa1-xN (x< 0.2). *Japanese Journal of Applied Physics, 39*(4B), L337.
[71] Tanaka, T., Watanabe, A., Amano, H., Kobayashi, Y., Akasaki, I., Yamazaki, S., & Koike, M. (1994). p-type conduction in Mg-doped GaN and $Al_{0.08}Ga_{0.92}N$ grown by metalorganic vapor phase epitaxy. *Applied physics letters*, *65*(5), 593-594.
[72] Suzuki, M., Nishio, J., Onomura, M., & Hongo, C. (1998). Doping characteristics and electrical properties of Mg-doped AlGaN grown by atmospheric-pressure MOCVD. *Journal of crystal growth*, *189*, 511-515.
[73] Han, S. H., Cho, C. Y., Lee, S. J., Park, T. Y., Kim, T. H., Park, S. H., ... & Park, S. J. (2010). Effect of Mg doping in the barrier of InGaN/GaN multiple quantum well on optical power of light-emitting diodes. *Applied Physics Letters*, *96*(5), 051113.
[74] Xie, J., Ni, X., Fan, Q., Shimada, R., Özgür, Ü., & Morkoç, H. (2008). On the efficiency droop in InGaN multiple quantum well blue light emitting diodes and its reduction with p-doped quantum well barriers. *Applied Physics Letters*, *93*(12), 121107.
[75] Ji, Y., Zhang, Z. H., Tan, S. T., Ju, Z. G., Kyaw, Z., Hasanov, N., ... & Demir, H. V. (2013).

Enhanced hole transport in InGaN/GaN multiple quantum well light-emitting diodes with a p-type doped quantum barrier. *Optics letters*, *38*(2), 202-204
[76] Shi, J. W., Sheu, J. K., Chen, C. H., Lin, G. R., & Lai, W. C. (2008). High-speed GaN-based green light-emitting diodes with partially n-doped active layers and current-confined apertures. *IEEE Electron Device Letters*, *29*(2), 158-160.
[77] Shi, J. W., Huang, H. Y., Sheu, J. K., Chen, C. H., Wu, Y. S., & Lai, W. C. (2006). The improvement in modulation speed of GaN-based Green light-emitting diode (LED) by use of n-type barrier doping for plastic optical fiber (POF) communication. *IEEE photonics technology letters*, *18*(15), 1636-1638.
[78] Otsuji, N., Fujiwara, K., & Sheu, J. K. (2006). Electroluminescence efficiency of blue In Ga N⁄ Ga N quantum-well diodes with and without an n-In Ga N electron reservoir layer. *Journal of Applied Physics*, *100*(11), 113105.
[79] Takahashi, Y., Satake, A., Fujiwara, K., Shue, J. K., Jahn, U., Kostial, H., & Grahn, H. T. (2004). Enhanced radiative efficiency in blue (In, Ga) N multiple-quantum-well light-emitting diodes with an electron reservoir layer. *Physica E: Low-dimensional Systems and Nanostructures*, *21*(2-4), 876-880.
[80] Hu, Z., Nomoto, K., Song, B., Zhu, M., Qi, M., Pan, M., ... & Xing, H. G. (2015). Near unity ideality factor and Shockley-Read-Hall lifetime in GaN-on-GaN pn diodes with avalanche breakdown. *Applied Physics Letters*, *107*(24), 243501.
[81] Maeda, T., Narita, T., Ueda, H., Kanechika, M., Uesugi, T., Kachi, T., ... & Suda, J. (2019). Shockley–Read–Hall lifetime in homoepitaxial p-GaN extracted from recombination current in GaN p–n+ junction diodes. *Japanese Journal of Applied Physics*, *58*(SC), SCCB14.
[82] Nguyen, H. P. T., Djavid, M., Cui, K., & Mi, Z. (2012). Temperature-dependent nonradiative recombination processes in GaN-based nanowire white-light-emitting diodes on silicon. *Nanotechnology*, *23*(19), 194012.
[83] Götz, W., Johnson, N. M., Chen, C., Liu, H., Kuo, C., & Imler, W. (1996). Activation energies of Si donors in GaN. *Applied Physics Letters*, *68*(22), 3144-3146.